NEGATIVE REFRACTION USING TRUE LEFT-HANDED METAMATERIALS

A THESIS
SUBMITTED TO THE DEPARTMENT OF PHYSICS
AND THE INSTITUTE OF ENGINEERING AND SCIENCE
OF BİLKENT UNIVERSITY
IN PARTIAL FULFILLMENT OF THE REQUIREMENTS
FOR THE DEGREE OF
MASTER OF SCIENCE

By

Koray Aydın

September, 2004

I certify that I have read this thesis and that in my opinion it is fully adequate, in scope and in quality, as a dissertation for the degree of Master of Science.

Prof. Dr. Ekmel Özbay (Supervisor)

I certify that I have read this thesis and that in my opinion it is fully adequate, in scope and in quality, as a dissertation for the degree of Master of Science.

Prof. Dr. Alexander Shumovsky

I certify that I have read this thesis and that in my opinion it is fully adequate, in scope and in quality, as a dissertation for the degree of Master of Science.

Assist. Prof. Dr. Vakur B. Ertürk

Approved for the Institute of Engineering and Science:

Prof. Dr. Mehmet Baray,
Director of the Institute of Engineering and Science

Abstract

NEGATIVE REFRACTION USING TRUE LEFT-HANDED METAMATERIALS

Koray Aydın
M. S. in Physics
Supervisor: Prof. Dr. Ekmel Özbay
September 2004

Left-handed materials and negative refraction attracted a great amount of attention in recent years due to their unique physical properties. It is possible to obtain a left-handed material by combining a novel artificial structure (split ring resonator) and a wire structure periodically. We investigated the transmission and reflection properties of split ring resonators (SRR), wires and composite metamaterials consisting of SRR and wire structures. We have successfully demonstrated true left-handed behavior in free space with a high transmission peak (-1.2 dB). This is the highest transmission peak reported for a left-handed material. The left-handed transmission band coincides exactly with the region where both dielectric permittivity and magnetic permeability have negative values. We proposed and demonstrated a new method to distinguish the magnetic resonance of the SRR structures.

We experimentally confirmed that composite metamaterial has a negative refractive index, at the frequencies where left-handed transmission takes place. Phase shift between consecutive numbers of layers of CMM is measured and phase velocity is shown to be negative at the relevant frequency range. Refractive index values obtained from the refraction experiments (-1.87) and the phase shift experiments (-1.78) are in good agreement.

Keywords*:* Left-Handed Material, Composite Metamaterial, Split Ring Resonator, Negative Permittivity, Negative Permeability, Effective Medium Theory, Photonic Band Gap, Negative Refraction, Negative Phase Velocity.

Özet

GERÇEK SOLAK MATERYALLER KULLANARAK NEGATİF KIRILMA ELDE EDİLMESİ

Koray Aydın
Fizik Yüksek Lisans
Tez Yöneticisi: Prof. Dr. Ekmel Özbay
Eylül 2004

Solak materyaller ve negatif kırılma kendilerine has fiziksel özellikleri dolayısıyla günümüzde oldukça ilgi çeken konular haline gelmişlerdir. Yeni bir yapay yapı olan yarıklı halka rezonatörleri ve ince tel yapıları kullanılarak solak materyal elde etmek mümkündür. Bu çalışmada yarıklı halka rezonatörleri, tel yapıları ve bu ikisinin bir araya getirilmesiyle oluşan karma ara-maddelerde geçirgenlik ve yansıma özelliklerini inceledik. Gerçek solak davranış sergileyen ve yüksek geçirgenliğe (-1.2 dB) sahip olan karma ara-maddeler başarıyla gösterildi. Bu geçirgenlik değeri bugüne kadar rapor edilmiş olan en yüksek değerdir. Solak geçirgenlik bandı hem dielektrik permitivite hem de magnetik permeabilitenin eksi değerler aldığı frekans bölgesinde yer almaktadır. Yarıklı halka rezonatörlerinin magnetik rezonansını belirleyebilmek için yeni bir metod geliştirdik ve bu metodu deneysel olarak da doğruladık.

Solak geçirgenliğin olduğu frekans aralığında karma ara-maddenin eksi kırılma indeksine sahip olduğunu deneysel olarak kanıtladık. İki farklı uzunluktaki karma ara-maddelerin faz farkı ölçülmek suretiyle, ilgili frekans aralıklarında bu yapıların eksi faz hızına sahip oldukları gösterildi. Kırılma deneyinden elde edilen kırılma indeksi (-1.87) ile faz farkından hesaplanan kırılma indeksi (-1.78) birbirlerine oldukça yakın değerlere sahiptirler.

***Anahtar Sözcükler**:* Solak Materyal, Karma Ara-Madde, Yarıklı Halka Rezonatörü, Negatif Permitivite, Negatif Permeabilite, Efektif Ortam Teorisi, Fotonik Bant Aralığı, Negatif Kırılma, Negatif Faz Hızı.

Acknowledgements

It is my pleasure to express my deepest gratitude and respect to Prof. Dr. Ekmel Özbay for his invaluable guidance, helpful suggestions and endless support. His personal and academic virtue shaped my academic personality and changed my approach to scientific study. I am very lucky to have the opportunity to study under his tutelage.

I would like to thank to the members of my thesis committee, Prof. Dr. Alexander Shumovsky and Assist. Prof. Dr. Vakur B. Ertürk, for reading the manuscript and commenting on the thesis.

Very special thanks to Dr. Mehmet Bayındır from whom I learnt a lot, including the importance of hard work. His invaluable advice and superior motivation during my difficult times kept me standing. I am also indebted to Ertuğrul Çubukçu for his help, understanding and friendship. I appreciate Dr. Kaan Güven for his great advice, endless help and continuous support during my research.

I would like to thank my office mates, Necmi Bıyıklı, İbrahim Kimukin, İrfan Bulu, Süheyla Sena Akarca Bıyıklı, Bayram Bütün, Hümeyra Çağlayan and Turgut Tut for creating a fruitful working environment. It is a great pleasure to work together with such nice and hardworking friends.

I am also thankful to my friends in the physics department, Muhammed Yönaç, Yavuz Öztürk, Rasim Volga Ovali, Serdar Özdemir, Levent Subaşı, Engin Durgun, Sefa Dağ, Aşkın Kocabaş, and Sinem Binicioğlu Çetiner. Your friendship is invaluable to me. And Emine "Abla", thank you as well, for making my life easier.

There is a long list of my close friends, whether old or new, far away of nearby; to feel their existence is my life source. Thank you all.

I would like to express my endless thanks to my mother, father and sister for their love, encouragement and care. I would also thank to my new family, who doubled the support and encouragement I have.

Finally, special thanks go to my wife, **Elif**, for her boundless love, endless trust and for shining a different color onto my life. I cannot imagine finishing all my achievements without her endless moral support. I dedicate this labor to her.

Contents

List of Figures

I do not know what I may appear to the world, but to myself I seem to have been only a boy playing on the sea-shore, and diverting myself in now and then finding a smoother pebble or a prettier shell than ordinary, whilst the great ocean of truth lay all undiscovered before me.

Isaac Newton

Chapter 1

Introduction

Left-handed materials and negative refraction phenomena have been studied extensively in recent years due to their unique physical properties and novel applications. Negative refraction of electromagnetic waves is the most interesting physical phenomena behind the left-handed metamaterial structures. The reversal of Doppler shift and backward Cerenkov radiation are also unusual physical characteristics arising from left-handed materials.

The electric and magnetic properties of materials are determined by two important material parameters, dielectric permittivity and magnetic permeability. Together the permeability and the permittivity determine the response of the material to the electromagnetic radiation. Generally, ε and μ are both positive in ordinary materials. While ε could be negative in some materials (for instance, ε posses negative values below the plasma frequency of metals), no natural materials with negative μ are known. However, for certain structures, which are called left-handed materials (LHM), both the effective permittivity, ε_{eff} and permeability, μ_{eff} possess negative values. In such materials the index of refraction, n, is less than zero, and therefore, phase and group velocity of an electromagnetic (EM) wave can propagate in opposite directions such that the direction of propagation is reversed with respect to the

direction of energy flow [1]. This phenomenon is called the negative index of refraction and was first theoretically proposed by Veselago in 1968, who also investigated various interesting optical properties of the negative index structures [1].

Negative effective permittivity in the microwave frequency range can be achieved by using periodic thin wire media. Dielectric permittivity takes negative values and EM waves cannot propagate inside the medium below the plasma frequency [2-4]. Electric charge is responsible for a large electric response in dielectric materials. Because of the lack of magnetic charge analogous to electric charge, it is more difficult to obtain a material with negative magnetic permeability. Pendry *et al.* suggested that a periodic array of artificial structures called split ring resonators (SRRs) exhibit negative effective μ for frequencies close to the magnetic resonance frequency [5]. Smith *et al.* reported the experimental demonstration of left-handed materials by stacking SRR and thin wire structures as arrays of 1D and 2D structured composite metamaterials (CMM). [6,7].

Theoretical calculations and analyses showed that the refractive index is indeed negative, where both ε and μ are simultaneously negative [1,8]. Experimental observation of negative refraction in left-handed materials is verified by Shelby *et al.* [9]. Negative refraction, and in general, wave propagation in negative index media have also been a controversial subject and have generated an intense debate. Valanju *et al.* claimed that dispersion implies positive refraction of group velocity even when the phase velocity is refracted negatively [10]. Effects of dispersion and loss on negative refraction experiments [11], and perfect lens behavior of left-handed materials [12] are

criticized. But further experimental studies on negative refraction, addressing the issues criticized, using different techniques supported the existence of negative refraction [13,14].

On the other hand, composite metamaterials (Fig 1.1(a)) are not the only materials that give rise to the negative refraction concept. Negative refraction is also achievable by using 2D photonic crystals (PCs) (Fig 1.1(b)). Theoretical studies [15-17] and experimental observations [18-20] confirmed the existence of the negative refractive index for 2D PCs. Negative refraction using 2D PCs has a different physical origin and the argument on negative values of ε and μ is not used. The equal frequency contours of PC and air, and the conservation of the parallel wave-vector component form the basis of the negative refraction idea in 2D photonic crystals [21].

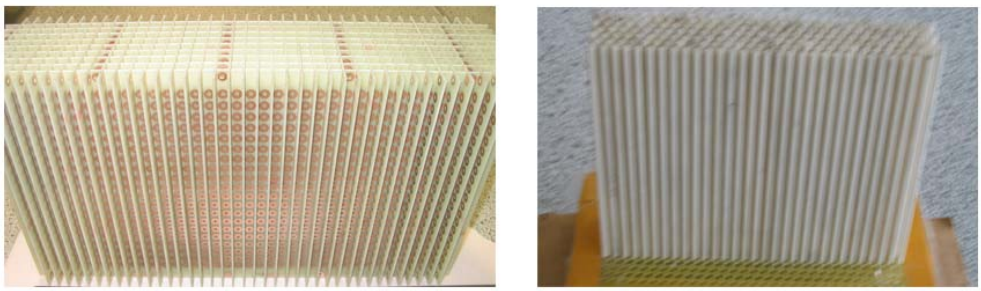

Fig 1.1: Examples of Negative refractive media (a) Left-handed metamaterials, (b) 2D Photonic Crystals.

Left-handed materials can be used in several applications. A perfect lens is a possible application. An unconventional alternative to a lens, a slab of negative refractive index material, has the power to focus all Fourier components of a

2D image, even those that do not propagate in a radiative manner [22]. Reversals of Doppler effect [23] and Cerenkov radiation[24], backward wave propagation[25], are the other interesting physical phenomena rising from the negative refractive concept. Moreover, structures with negative μ, can be used for magnetic resonance imaging [26].

This thesis will be organized as follows. In the second chapter, we will have a theoretical introduction to left-handed materials and its components. We will discuss how to achieve negative permittivity and negative permeability at the microwave frequency range. Later we will show how to obtain a negative refractive index medium, using negative permittivity and negative permeability media together. In the third chapter, the transmission characteristics of SRRs, wires and CMMs in free space will be considered. Most of the work presented in chapter 3 appeared as a journal article in IEEE Transactions on Antennas and Propagation [27].

In chapter 4, we first identify the magnetic resonance and electric resonance of SRRs by using ring resonators with the splits closed. We then verify the effect of the interaction between SRRs and wires and demonstrate experimentally the shift in plasma frequency. Finally we present a new CMM structure that exhibits true left-handed behavior and has a transmission band with a peak value at -1.2 dB. Some of the achievements represented in chapter 4 are to appear as a journal article in Optics Letters [28]. In chapter 5, we demonstrate a negative refractive index in left-handed metamaterials. Then we present direct experimental evidence that the phase velocity is negative within the left-handed pass band of a CMM. Some of the contents of chapter 5 have been submitted to Applied Physics Letters [29]. The last chapter will include a

brief summary of the results obtained during this thesis work. Future perspectives and directions will also be provided in this chapter.

Chapter 2

Theoretical Background

2.1 Introduction

The dielectric constant ε and the magnetic permeability μ are the fundamental characteristic quantities that determine the propagation of electromagnetic waves in matter. This is due to the fact that they are the only material parameters appearing in the dispersion equation

$$\left| \frac{\omega^2}{c^2} \varepsilon_{ij} \mu_{ij} - k^2 \delta_{ij} + k_i k_j \right| = 0 \tag{2.1}$$

which gives the relation between the frequency ω of a monochromatic wave and its wave vector k. For an isotropic substance Eq. (2.1) takes a simpler form:

$$k^2 = \frac{\omega^2}{c^2} n^2 \tag{2.2}$$

where n^2 is given by

$$n^2 = \varepsilon\mu \tag{2.3}$$

From Eqs. (2.2) and (2.3), one can say that a simultaneous change of the signs of ε and μ has no effect on these relations [1]. But as we will see in the upcoming parts of this chapter, materials having simultaneously negative

values of ε and μ have some physical properties and unique characteristics that are different from those of ordinary materials having positive ε and μ.

To understand the effect of changes in the signs of ε and μ, we have to consider the initial Maxwell equations, where ε and μ appear separately, different from equations Eqs. (2.1), (2.2) and (2.3) where their product appears in the equations [1]. Primarily Maxwell equations

$$\begin{aligned} \nabla \text{ x } \mathbf{E} &= -\frac{1}{c}\frac{\partial \mathbf{B}}{\partial \mathbf{t}} \\ \nabla \text{ x } \mathbf{H} &= \frac{1}{c}\frac{\partial \mathbf{D}}{\partial \mathbf{t}} \end{aligned} \tag{2.4}$$

and constitutive relations

$$\begin{aligned} \mathbf{B} &= \mu \mathbf{H} \\ \mathbf{D} &= \varepsilon \mathbf{E} \end{aligned} \tag{2.5}$$

are given. For a monochromatic plane wave, all quantities are proportional to $e^{i(kz-\omega t)}$ and therefore Eqs. (2.4) and (2.5) reduce to

$$\begin{aligned} \mathbf{k} \text{ x } \mathbf{E} &= \frac{\omega}{c}\mu \mathbf{H} \\ \mathbf{k} \text{ x } \mathbf{H} &= -\frac{\omega}{c}\varepsilon \mathbf{E} \end{aligned} \tag{2.6}$$

These are the key expressions to understand the problem of left-handed materials. If both ε and μ are positive, it is clearly seen that **E**, **H** and **k** form a right-handed triplet of vectors. The interesting point is that for simultaneously negative values of ε and μ, a left-handed vector triplet of **E**, **H** and **k** is formed. At the same time, the direction of the energy flow determined by the Poynting vector **S** is independent of the signs and values of ε and μ:

$$\mathbf{S} = \frac{c}{4\pi}\mathbf{E} \text{ x } \mathbf{B} \tag{2.7}$$

Poynting vector is always directed away from the source of the radiation. But amazingly the **k** vector may be directed away from the source (for the cases where ε and μ are both positive) or towards the source (for the cases where ε and μ are both negative). This is the major difference between the case with negative ε and μ values and the case with corresponding positive values [1].

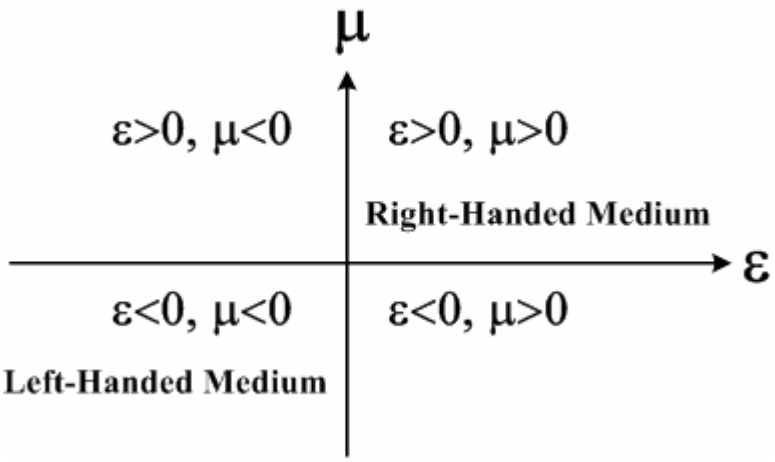

Figure 2.1: ε and μ space. 3rd region shows left-handed medium.

Figure 2.1 shows ε and μ space. Ordinary materials having $\varepsilon > 0$ and $\mu > 0$ allow the propagation of EM waves, and they have positive refractive index values hence they can be called right-handed media. Since one of the permittivity or permeability values is negative and the other is positive at the second and fourth parts of ε and μ space, EM waves cannot propagate inside the medium and evanescent waves will occur. For the third part of the ε and μ space, since the product of ε and μ are positive, EM waves can propagate inside

the medium. This part is the left-handed media part, since both ε and μ are simultaneously negative as will be discussed later in this chapter.

2.2 Negative Permittivity ($\varepsilon < 0$)

Plasma is a medium with an equal concentration of positive and negative charges, of which at least one charge type is mobile. In a solid, the negative charges of the conduction electrons are balanced by an equal concentration of positive charge of the ion cores [30].

The polarization of a collection of atoms or molecules can rise in two ways: a) The applied field distorts the charge distributions and so it produces an induced dipole moment in each molecule; b) the applied field tends to line up the initially randomly oriented permanent dipole moments of the molecules. To estimate the induced moments we consider a simple model of harmonically bound charges (electrons and ions) [31]. Each charge e is bound under the action of a restoring force

$$\mathbf{F} = -m\omega_0^2\mathbf{x} \tag{2.8}$$

where m is the mass of the charge, and ω_0 is the frequency of oscillation about equilibrium. The equation of motion for an electron of charge $-e$ bound by a harmonic force (Eq. 2.8) and acted by an electric field $\mathbf{E}(\mathbf{x},t)$ is given by

$$m\left[\ddot{\mathbf{x}} + \gamma\dot{\mathbf{x}} + \omega_0^2\mathbf{x}\right] = -e\mathbf{E}(\mathbf{x},t) \tag{2.9}$$

where γ is a damping term representing dissipation of the plasmon's energy into the system. An approximation can be made taking into account that the amplitude of the oscillation is small enough to permit the evaluation of the

electric field at the average position of the electron. If the field varies harmonically in time with the frequency ω as $e^{-i\omega t}$, the dipole moment contributed by one electron is

$$\mathbf{p} = -e\mathbf{x} = \frac{e^2}{m}(\omega_0^2 - \omega^2 - i\omega\gamma)^{-1}\mathbf{E} \tag{2.10}$$

If we suppose that there are N molecules per unit volume with Z electrons per molecule, and that, instead of a single binding frequency for all, there are f_j electrons per molecule with a binding frequency ω_j and damping constant γ_j, then the dielectric constant is given by [31]

$$\frac{\varepsilon(\omega)}{\varepsilon_0} = 1 + \frac{Ne^2}{\varepsilon_0 m}\sum_j f_j(\omega_j^2 - \omega^2 - i\omega\gamma_j)^{-1} \tag{2.11}$$

At frequencies far above the highest resonant frequency the dielectric constant takes on the simplest form

$$\varepsilon(\omega) = 1 - \frac{\omega_p^2}{\omega(\omega + i\gamma)} \tag{2.12}$$

which is approximately independent of the wave vector, **k**. The significant point about Eq. (2.12) is that, $\varepsilon(\omega)$ is essentially negative below the plasma frequency (ω_p), at least down to frequencies comparable to γ. A longitudinal mode, the plasmon, appears at a fixed frequency, and two longitudinal modes emerge at the plasma frequency. In consequence of the negative ε, only evanescent modes (imaginary wave vector) exist below the plasma frequency and below this threshold no radiation penetrates very far into the metal [2].

The frequency ω_p, which depends only on the total number of $n = NZ$ of electrons per unit volume is given by the formula

$$\omega_p^2 = \frac{ne^2}{\varepsilon_0 m_{eff}} \tag{2.13}$$

In simple metals γ is small relative to ω_p. For instance $\omega_p = 15$ eV whereas $\gamma = 0.1$ eV for aluminum [2].

The electromagnetic response is dominated by negative permittivity concept in the visible and UV frequency regions. However, at lower frequencies starting from the near infrared and downwards, dissipation asserts itself, therefore dielectric function becomes imaginary. To achieve negative permittivity values at microwave range, the thin metallic wire concept is proposed [2,3]. Also loop-wire medium is investigated for the same purposes [4].

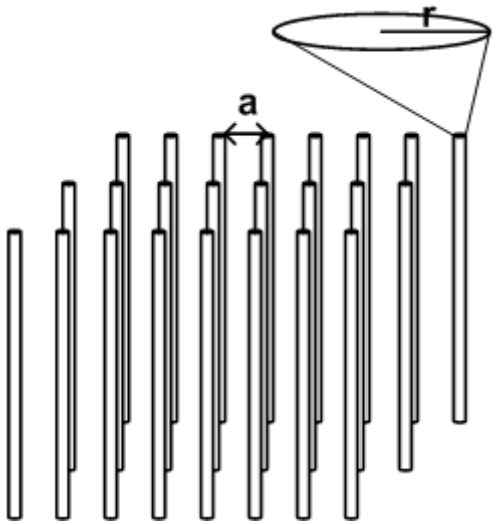

Figure 2.2: A periodic configuration of thin metallic wires with a lattice spacing of *a* and radius *r*.

By assembling thin metallic wire structures into a periodic medium (Fig 2.2) with appropriate parameters, negative permittivity can easily be achieved at microwave frequencies. Plasma frequency of the thin metallic wires is given after detailed calculations as [2]

$$\omega_p^2 = \frac{ne^2}{\varepsilon_0 m_{eff}} = \frac{2\pi c_0^2}{a^2 \ln(a/r)} \tag{2.14}$$

where c_0 is the speed of light in free space, a is the lattice parameter and r is the radius of the wires.

Note that although the newly reduced plasma frequency can be expressed in terms of electron effective mass and charge, these microscopic quantities cancel, leaving a formula containing only macroscopic parameters of the system: radius of the wires, and periodicity of the wire medium.

The metallic wires were structured on a scale much less than the wavelength of radiation. When the wavelength of the incident radiation is much larger than the size and spacing of a collection of scatterers, the response of the scatterers to the incident fields can be treated by way of the effective medium theory.

$$a << \lambda = 2\pi c_0 \omega^{-1} \tag{2.15}$$

In the thin wire case, the effective medium theory holds since corresponding λ for ω_p is much larger than the radius of the wires. Therefore, an effective dielectric permittivity, ε_{eff} can be used to define the permittivity of the medium. As far as external electromagnetic radiation is concerned, a thin wire structure appears as an effectively homogeneous dielectric medium whose internal structure is only apparent as it dictates ε_{eff}. In this respect it is important that the

structure be made of thin wires. Eq. (2.14) shows that the function of the small radius is to suppress the plasma frequency. For a thick wire structure in Eq. (2.14), $\ln(a/r)\approx 1$ so that the plasma frequency corresponds to a free space wavelength of approximately twice the lattice spacing. Therefore, Bragg diffraction effects would interfere with our simple plasmon picture. Choosing a small radius ensures that diffraction occurs only at much higher frequencies.

2.2 Negative Permeability ($\mu < 0$)

Electric charge is responsible for large electric response in dielectric materials. Because of the lack of magnetic charge analogous to an electric charge, it is more difficult to obtain a material with negative magnetic permeability. Naturally occurring materials almost universally have a positive permeability, and thus a left-handed material, while not ruled out by fundamental considerations, seemed unlikely to be practical. However, in 1999, Pendry *et al.* [5] introduced several configurations of conducting scattering elements displaying a magnetic response to an applied electromagnetic field when grouped into an interacting periodic array.

Usually the magnetic permeability equals to unity ($\mu = 1$) for ordinary materials. Thin metallic wire media discussed in the previous section of this chapter responds to the electric field and dielectric permittivity becomes negative below the plasma frequency of the wires. But these metallic wire structures do not give any response to the magnetic field. So in order to obtain negative permeability, one has to extend the magnetic properties of the materials. Pendry *et al.* [5], enhanced the magnetic response of artificially designed materials by introducing capacitative elements into the structure.

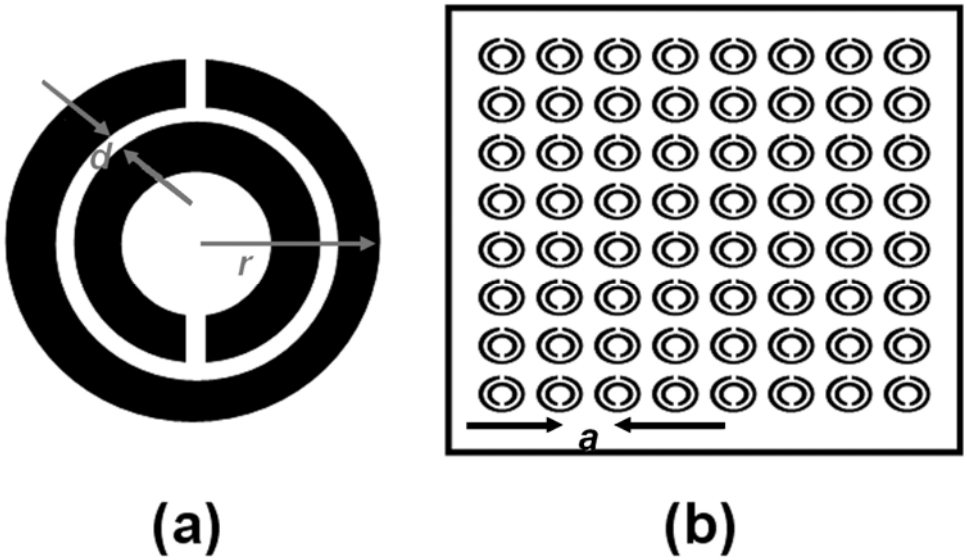

Figure 2.3: Schematic drawings of (a) Single split ring resonator (SRR) (b) SRRs grouped into a periodic array.

Figure 2.3(a) shows the design of Pendry, described as a split ring resonator (SRR) [5]. In a split ring resonator there are two rings both having a split. By having splits in the rings, the SRR unit can be made resonant at wavelengths much larger than the diameter of the rings. The purpose of the second split ring, inside and whose split is oriented oppositely to the outside split, is to generate a large capacitance in the small gap region. The gap between the rings prevents current from flowing around any one ring. However, there is a considerable capacitance between the two rings, which enables current to flow. By combining the SRRs into a periodic medium, (Fig. 2.3(b)) such that there is strong magnetic coupling between the resonators, unique properties emerge from the composite and isotropy can be achieved.

Structures having effective permeability and permittivity comply with the following equation

$$\begin{aligned} \mathbf{B}_{\text{ave}} &= \mu_{\text{eff}}\mu_0\mathbf{H}_{\text{ave}} \\ \mathbf{D}_{\text{ave}} &= \varepsilon_{\text{eff}}\varepsilon_0\mathbf{E}_{\text{ave}} \end{aligned} \tag{2.16}$$

where we assume that the structure is on a scale much shorter than the wavelength of any radiation, in order to enable the ability for us to talk about an average value for all of the fields.

Detailed calculations [5] give effective permeability of the SRR to be

$$\mu_{\text{eff}} = 1 - \frac{F}{1 + \frac{2\sigma i}{\omega r \mu_0} - \frac{3}{\pi^2 \mu_0 \omega^2 C r^3}} \tag{2.17}$$

where F is the fractional volume of the cell, and r is the radius of the outer ring

$$F = \frac{\pi r^2}{a^2} \tag{2.18}$$

C is the capacitance per unit area, and a is the lattice constant,

$$C = \frac{\varepsilon_0}{d} = \frac{1}{dc_0^2\mu_0} \tag{2.19}$$

where d is the distance between the split rings. Hence

$$\mu_{\text{eff}} = 1 - \frac{\frac{\pi r^2}{a^2}}{1 + \frac{2\sigma i}{\omega r \mu_0} - \frac{3dc_0^2}{\pi^2 \omega^2 r^3}} \tag{2.20}$$

Since a capacitance is introduced into the system, effective permeability of the SRR becomes resonant. Figure 2.4 illustrates the generic form of μ_{eff} for SRRs.

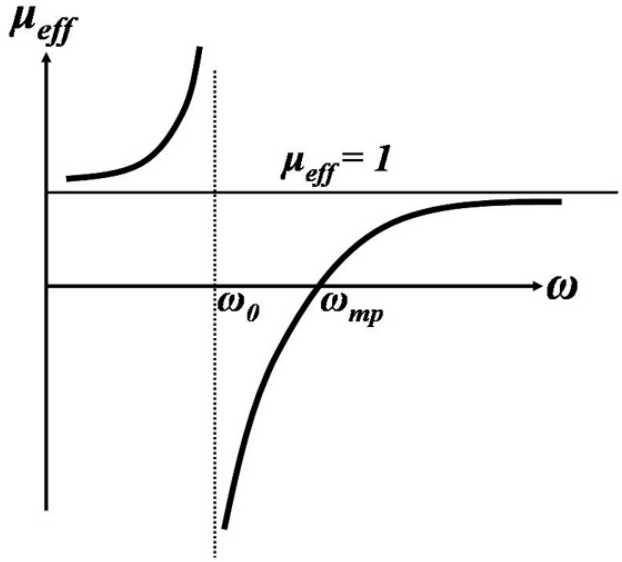

Figure 2.4: Resonance for effective permeability of SRRs [5].

ω_0 is defined to be the frequency at which μ_{eff} diverges as follows:

$$\omega_0 = \sqrt{\frac{3}{\pi^2 \mu_0 C r^3}} = \sqrt{\frac{3dc_0^2}{\pi^2 r^3}} \tag{2.21}$$

and ω_{mp} to be the magnetic plasma frequency

$$\omega_{mp} = \sqrt{\frac{3}{\pi^2 \mu_0 C r^3 (1-F)}} = \sqrt{\frac{3dc_0^2}{\pi^2 r^3 (1-\frac{\pi r^2}{a^2})}} \tag{2.22}$$

Pendry *et al.* carried through this analysis, finding a generic function for the effective permeability

$$\mu_{\text{eff}} = 1 - \frac{F\omega^2}{\omega^2 - \omega_0^2 + i\Gamma\omega} \tag{2.20}$$

Eq. (2.20) indicates that propagating modes occur up until the frequency ω_0, followed by a gap where no propagating modes exist, followed by propagating modes starting from the frequency $\omega_0 / \sqrt{1-F}$. The reason for the gap in propagation is of particular significance, since effective permeability will become negative for this frequency region. Turning back to Fig. 2.4, the real part of the permeability increases from unity at $\omega = 0$ to a large positive values near $\omega = \omega_0$, where it then abruptly passes to a large negative value, crossing $\mu = 0$ at $\omega = \omega_{mp}$. The peak value of the permeability, infinite in the case of no loss, is constrained by the magnitude of the material loss in the SRR [32]. The width of the negative permeability region is determined by the filling factor F (Eq. 2.18). At high frequencies Eq. (2.20) implies that the permeability tends toward 1-F, however, it is understood that the material will stop responding at a very high frequency, and the permeability will actually reach unity.

The polarization of the electromagnetic field with respect to the SRR structure is a key issue to achieve negative values of μ_{eff}. There are two incident polarizations of interest: magnetic field along the split ring axes, $H_{\parallel}$ case (Fig. 2.5.(a)) and perpendicular to the split ring axes, $H_{\perp}$ case (Fig 2.5.(b)). In both cases, the electric field is in the plane of the rings. Measurements and analyses showed that there are stop bands for both polarization cases where EM waves cannot propagate inside the medium [6]. A photonic band gap of the SRR medium does not necessarily imply that μ_{eff} is negative. Therefore one has to check whether the gap is due to negative μ_{eff} or negative ε_{eff} of the structures.

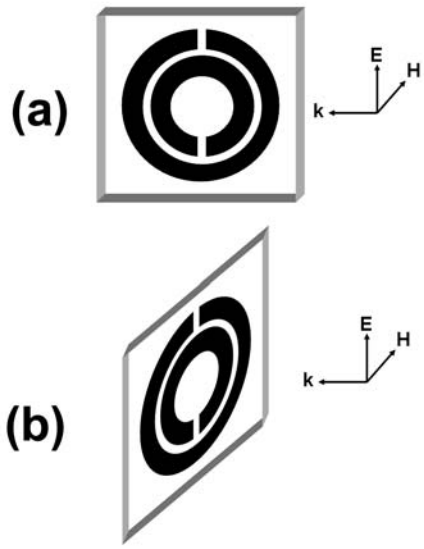

Figure 2.5: Magnetic field polarized (a) along the split ring axis, $H_{\parallel}$ case, (b) perpendicular to the split ring axis, $H_{\perp}$ case.

Smith *et al.* investigated the reason of the gap by altering the dielectric function of the medium and creating scattering properties that can distinguish whether the band gaps are due to either the μ_{eff} or ε_{eff} of SRR being negative [6,33]. It is shown that for $H_{\parallel}$ case, SRRs respond to magnetic field and μ_{eff} becomes negative over a certain frequency range. But for the $H_{\perp}$ case, magnetic effects are small, and μ_{eff} varies slowly and thus have a small and positive μ_{eff} value [6]. Since the SRR structures in Fig. 2.5 are designed to be 1-Dimensional elements, we have anisotropic material. To obtain negative permeability for each polarization, one should use higher dimension SRR structures, to lift off the anisotropy of the 1D SRR structures. In chapter 4, we will show an alternative and easier way to determine the formation of band gaps of the SRRs.

2.4 Negative Refraction

Maxwell equations determine how electromagnetic waves propagate within a medium and can be solved to arrive at a wave equation of the form

$$\frac{\partial^2 E(x,t)}{\partial x^2} = \varepsilon\mu \frac{\partial^2 E(x,t)}{\partial t^2} \tag{2.21}$$

In Eq. 2.21 ε and μ enter as a product, so it is not a problem whether both their signs are positive or negative. Indeed solutions have the form of $\exp[i(nkd - \omega t)]$, where $n = \sqrt{\varepsilon\mu}$ is the refractive index. Propagating solutions exist in the material for two distinct cases: i) $\varepsilon > 0$ and $\mu > 0$, ii) $\varepsilon < 0$ and $\mu < 0$. So, what is the difference between positive and negative refractive indices, and why do we choose n to be negative?

Let us consider the refraction phenomena occurring when an incident beam transits from one medium into another. Suppose that the initial has a positive refractive index, therefore $\varepsilon_1 > 0$ and $\mu_1 > 0$. If $\varepsilon_2 > 0$ and $\mu_2 > 0$, we shall have an ordinary refraction case. But for the case where $\varepsilon_2 < 0$ and $\mu_2 < 0$, we have a beam transition from an ordinary medium into a medium with negative ε and μ. However, in every case the boundary conditions should be reached. Remember that boundary conditions require tangential components of **E** and **H,** and normal components of **D** and **B** to be continuous at the interface.

$$E_{t_1} = E_{t_2} \quad , \quad H_{t_1} = H_{t_2} \tag{2.22}$$

$$\varepsilon_1 E_{n_1} = \varepsilon_2 E_{n_2} \quad , \quad \mu_1 H_{n_1} = \mu_2 H_{n_2} \tag{2.23}$$

It is evident from Eqs. (2.22) and (2.23) that x and y components of the field are not changed at transition from medium 1 to 2, regardless of the signs of ε and μ. As for the normal z components of the field, they preserve their directions if ε and μ preserve their signs in both media; they change their directions if two media have different signs of ε and μ [1].

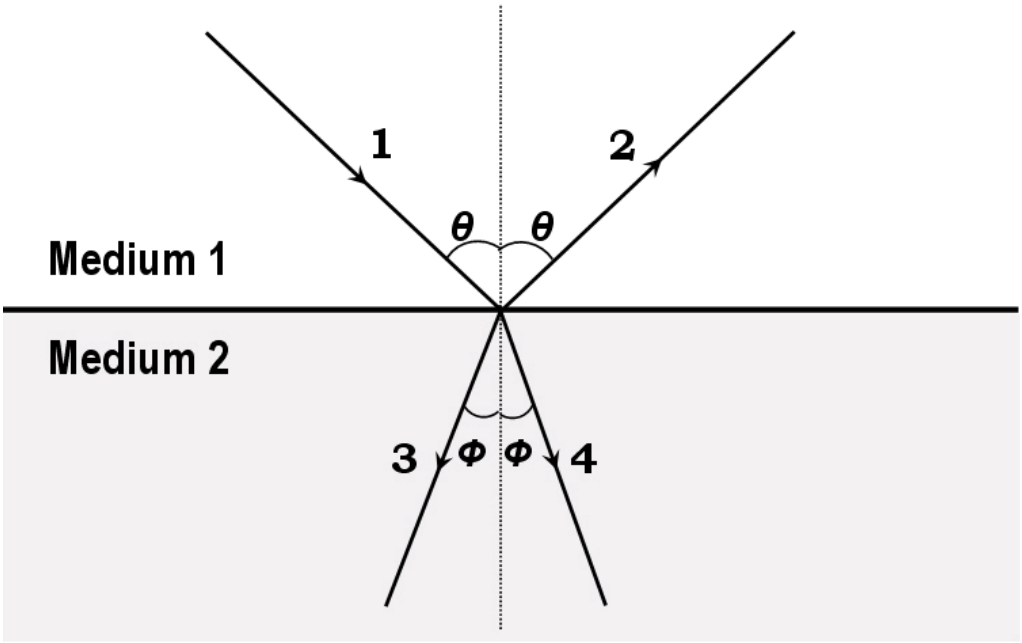

Figure 2.6: Schematic drawing of incident (1), reflected (2), negatively refracted (3) and positively refracted (4) beams.

If we consider relations (Eq. 2.6) with due reference to Eq. (2.22) and (2.23), it is immediately understood that a beam transition from a medium with positive ε and μ into a medium $\varepsilon < 0$ and $\mu < 0$, the sign of z component of k (k_z) is reversed. The sign reversal of k_z vector corresponds to a mirror reflection of a triad, **E**, **H** and **k** in the boundary plane of two media. This means that if a

beam goes from an ordinary medium into one with negative ε and μ, it is symmetrical compared to the case with positive ε and μ. In other words an incident beam is refracted at the other side of the normal, which is different than the case in an ordinary refraction. Figure 2.6 sketches the path of the beams when beam 1 is transiting from medium 1 to 2. There are four beam paths as seen in the figure: 1-incident beam, 2-reflected beam, 3-refracted beam when $n_2 < 0$, 4- refracted beam when $n_2 > 0$. If the beam is assumed to be incident to medium 1 at angle θ, the refraction angle Φ will be negative when ε_2 and μ_2 are both negative. Refractive index, n, determined by using Snell's law

$$n_1 \sin\theta = n_2 \sin\Phi \tag{2.24}$$

is also negative.

One needs to be careful when taking the square root of Eq. 2.3, because ε and μ are analytic functions whose values are generally complex. The ambiguity in the sign of the square root can be resolved with a proper analysis of the problem. Consider that we have a material having $\varepsilon = \mu = -1$. ε and μ can be written in another form as $\varepsilon = \exp(i\pi)$ and $\mu = \exp(i\pi)$, then $n = \sqrt{\varepsilon\mu} = \exp(i\pi/2)\exp(i\pi/2) = \exp(i\pi) = -1$. The important step is that the square root of either ε or μ alone must have a positive imaginary part, which is a necessity for passive material [34].

The $n < 0$ solution consists of plane waves propagating toward the source, rather than plane waves propagating away from the source. Since such a solution would normally be rejected on the grounds of causality, a general

method is employed by Smith *et al* [8]. The work done by the source on the fields is given[8] as

$$P = \Omega W = -\frac{1}{2}\int_V j^* E(x,\Omega)dx = \pi \frac{\mu}{cn} j_0^2 \qquad (2.25)$$

We require that the average work (W) done by source on the fields is positive. In a right-handed medium, both μ and n are positive, therefore $n > 0$ solution is selected. On the other hand, in a left-handed medium since $\mu < 0$, we conclude that the solution with $n < 0$ leads to the correct interpretation that the current performs positive work on the fields [8]. Since the work done by the source on the fields is positive, energy propagates outward from the source, in agreement with Veselago's proposals [1].

Negative refractive materials are necessarily frequency dispersive, so that the various frequency components of a modulated beam are refracted at different angles within the medium. Through an analysis of the points of the constant phase of a modulated plane wave, it is shown that both the group and phase velocities undergo negative refraction at the interface between a positive and a negative index material [35]. The interference fronts of the modulated wave are not normal to the group velocity, and exhibit a sideways motion as they move at the group velocity. Consideration of a modulated beam of finite extent clearly resolves the difference between the group velocity and normal to the interference fronts.

Existence of a negative refractive index implies an entirely new form of geometrical optics. A striking example is shown in Fig. 2.7(a), where a slab of

negative index material focuses the point source, which is not the case in the positive index materials. A rectangular lens made of positive index material will expectedly diverge the beam. But it is possible to focus EM waves using rectangular slab lenses made of left-handed materials. As seen in Fig. 2.7(a), EM waves cross inside the LHM slab lens (if the slab is thick enough), which implies a second focusing point, a different behavior from that of focusing in positive refractive materials. Fig. 2.7(b) shows the case when a convex lens of left-handed material is used. Different from the case in right-handed materials, waves diverge instead of converging. Fig. 2.7(c) is the case when a concave lens is used. Instead of a diverging beam, a converging beam is obtained.

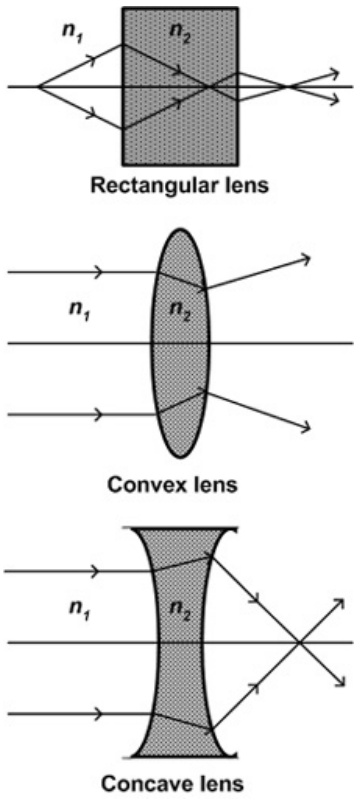

Fig 2.7: Beam path in (a) rectangular, (b) convex, (c) concave lenses made of left-handed materials.

If the permittivity and permeability and therefore refractive index is equal to -1, and the point source is close enough to the slab of a left-handed medium, impedance will be matched and therefore no reflection will occur. A slab can be designed to focus not only propagating waves, but also evanescent waves using left-handed materials. Such lenses are called “perfect lenses” [22]. Light can be brought to perfect focusing without the usual constraints imposed by the wavelength. Negative refractive index materials restore not only the phase of propagating waves, but also the amplitude of evanescent states.

Chapter 3

10 GHz Composite Metamaterials

3.1 Introduction

Left-handed materials were first proposed by Veselago at 1968 [1]. At year 2000 experimental evidence came by way of Smith *et al* [6]. Since the original microwave experiment by Smith *et al.*, several CMMs were fabricated that exhibited a pass band in which it was thought that both ε and μ were negative [7,36-44]. This assumption was based on transmission measurements of the wires alone, the SRRs alone and the CMM. The occurrence of a CMM transmission peak within the stop bands of the SRRs-only and wires-only structures was taken as evidence for left-handed behavior. Besides the experiments, there is also a large amount of numerical work in which transmission and reflection data, losses and absorptions and effective parameters of the composite metamaterials have been investigated [45-59].

In this chapter we investigate the transmission and reflection characteristics of CMMs in the microwave frequency range. Most of the previous experimental measurements were performed in a wave guide chamber, but our

measurements take place in free space. First we will have a look at the transmission and reflection characteristics of periodic wire medium alone. Then we will investigate the characteristics of periodic SRR structures. Later we will assemble SRR and wire media together in a periodic array to investigate the transmission and reflection characteristics of the CMM.

3.2 Transmission and Reflection Experiments

3.2.1 Experimental Setup

The transmission, reflection, and phase measurements of composite metamaterial structures are performed in free space by using a HP 8510C network analyzer. HP 8510 C network analyzer is capable of measuring both amplitude and phase. Experimental setup for transmission measurements is given in Fig. 3.1. A microwave horn antenna connected to a network analyzer transmits continuous electromagnetic waves at specific microwave frequency range depending on the waveguide size of the antenna. The other horn antenna measures the transmission, phase, group delay and photon lifetime parameters. In our experiments, normalization of the transmission is done as follows. First we measured the transmission spectra in the free space (i.e. without periodic structures). This data was used as the calibration data for the network analyzer. Then, we inserted the periodic structures between the horn antennas, and we performed the transmission measurements by maintaining distance between the transmitter and receiver horn antennas fixed. The distance between the horn antennas is kept at 40 cm for all measurements to get rid of near field effects.

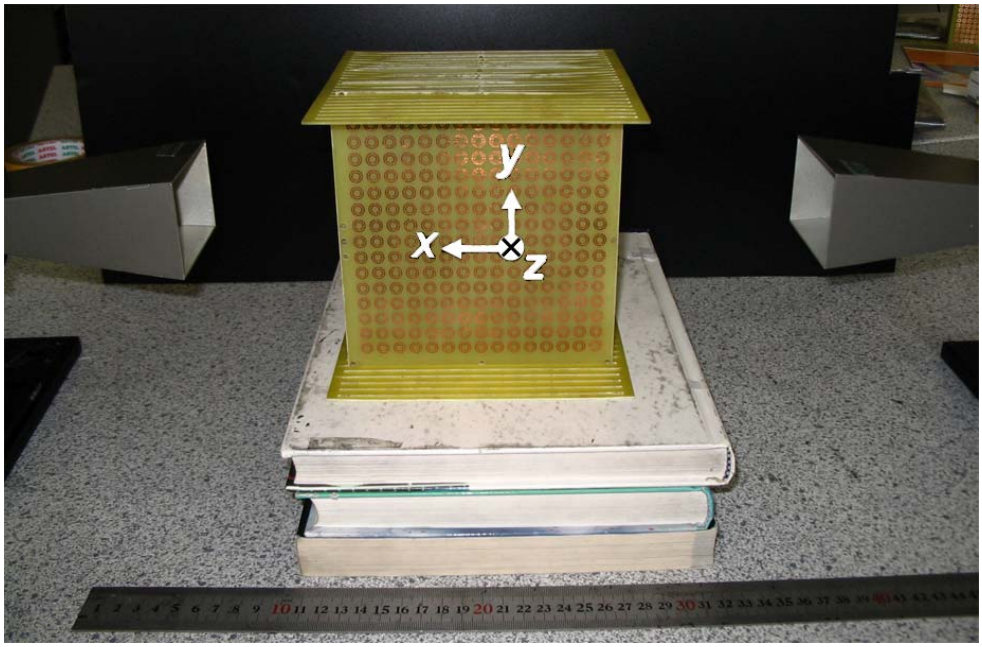

Fig 3.1: Experimental setup for transmission measurements.

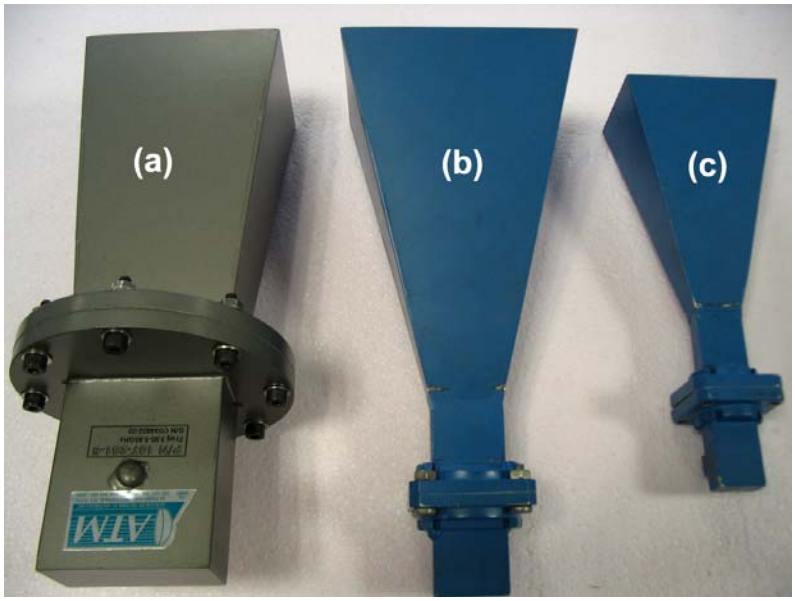

Fig 3.2: Horn antennas used to scan frequency regions (a) 3-7 GHz, (b) 7-14 GHz, (c) 10-22 GHz.

We scanned the frequency region 4-22 GHz, and for this purpose, we used a set of microwave horn antennas having various sizes. The antennas in Fig. 3.2(a) scans 4-7 GHz, Fig. 3.2(b) scans 7-14 GHz, and Fig 3.2(c) scans 10-22 GHz.

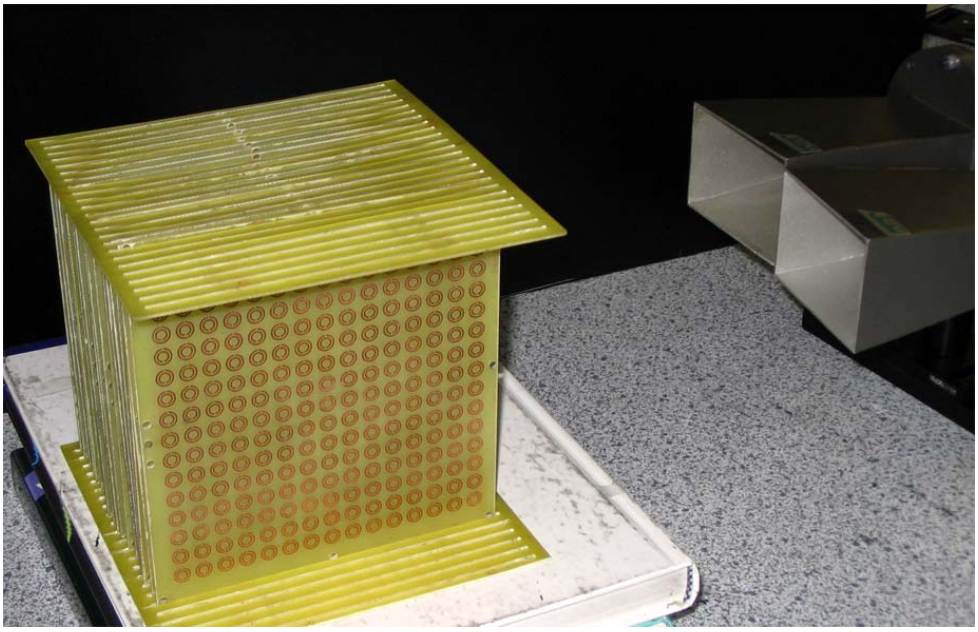

Fig 3.3: Experimental setup for reflection measurements

For reflection measurements, we used a different setup as shown in Fig 3.3. In this case two horn antennas are placed close to each other. The angle between the antennas is kept very small. The transmitter horn antenna sends the EM wave to the surface and the receiver antenna measures the amplitude of the reflected EM waves. Normalization of the reflection is also different from that of the transmission. Instead of measuring the spectra in free space, we placed a thick slab of metal (metals reflect all of the incident EM waves) at a proper distance away from the antennas. This data was used as the calibration

data for the network analyzer. Then we inserted the periodic structures by paying attention to the fact that the reflection surface of the structure is the same with the reflection surface of the thick metal used for calibration data. Microwave transmission measurements are performed in free space, which does not impose any restriction on the size of the structures. For all measurements, EM waves propagate along the *x* direction. The electric field polarization is along the *y* direction and magnetic field polarization is along the *z* direction. The directions are shown in Fig. 3.1.

3.2.2 Structures

In our experiments we used planar geometry of SRRs and wires. SRRs and wires are deposited on commercialy available printed circuit boards (PCB). PCB boards consisting of SRR arrays (Fig. 3.4(a)) and wire arrays (Fig. 3.4(b)) are ordered to a PCB firm. In all of the experiments performed in the content of this thesis work, we used the same kind of PCB boards. The dielectric constant and thickness of this dielectric boards are measured to be ε_b=4.4 and 1.6 mm, respectively. The deposited metal is copper and has a thickness of 30 μm. Losses are one of the largest problems for left-handed materials. To address the loss and absorption issue of empty PCB boards we measured the transmission spectrum of these boards. We put 20 layers of boards together, which correspond to a length of 3.2 cm in the propagation direction. Average transmission is measured to be around - 2.5 dB at the frequency range that we were interested in, which corresponds to ~ 60% transmission of EM waves. The PCB boards has n = 2.15, by using the formula

$R = (n\text{-}1)^2 / (n\text{+}1)^2$, reflection is calculated to be around ~ 15%. Therefore, ~ 25% of EM wave is absorbed by the bulk PCB boards.

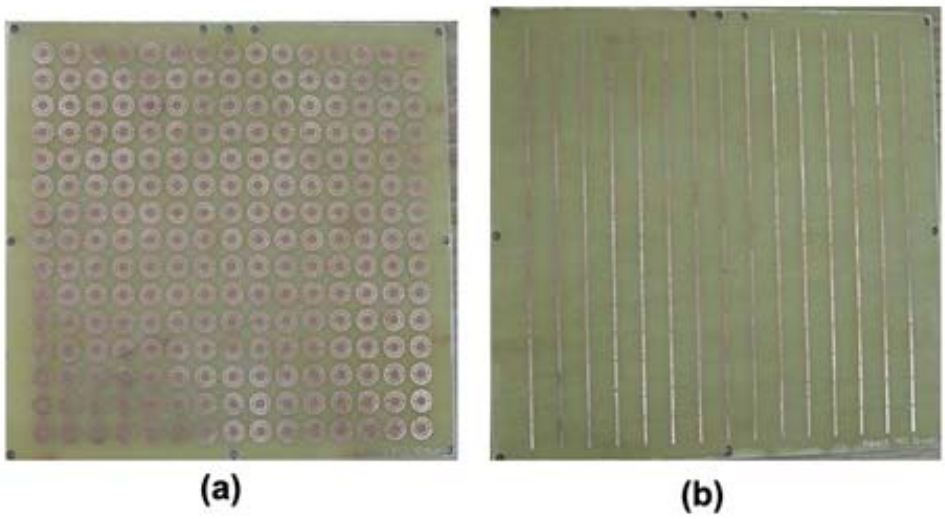

Fig. 3.4: Pictures of PCB boards consisting of (a) 15x15 SRR array, (b) 15x15 discontinuous wire array.

3.3 Transmission and Reflection Characteristics

3.3.1 Periodic "Discontinuous Thin Wire" Medium

A negative permittivity medium in the microwave frequency range can be achieved by arranging thin metallic wires periodically [2-4]. The continuous wire structure behaves like a high-pass filter, which means that the effective permittivity will take negative values below the plasma frequency [60].

However, for discontinuous wire structures, the negative permittivity range does not extend to zero frequency, and a stopband appears around the resonance frequency. In the microwave experiments performed by Smith *et al.*, [6,7] although the wires are continuous, because of the finite length of the wires (1 cm), there is a lower edge for the negative permittivity region. For this purpose, we used discontinuous wires instead of continuous wires.

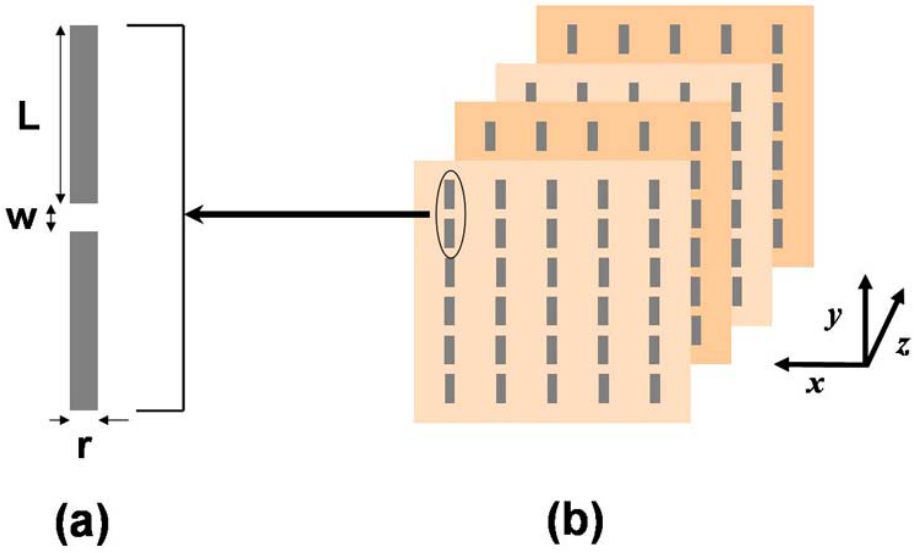

Fig. 3.5: Schematic drawings of (a) two wire strips separated by a gap, (b) periodical arrangement of discontinuous wire strips.

The thin wire crystal is constructed by depositing discontinuous wire strips, of length L = 8.65 mm, on the circuit board (Fig. 3.5(a)). The thickness of the stripes is r = 0.9 mm and the gap between the two stripes is w = 0.35 mm. The thickness of the wires is 30 μm. As shown in Fig. 3.5(b), the thin wire stripes with parameters N_x = 15, N_y = 15, and N_z = 20 units cells are stacked along

each direction. The periodicity along *x*, *y*, and *z* axes are a_x = 8.8 mm, a_y = 8.8 mm, and a_z = 6.5 mm, respectively.

The measured transmission and reflection characteristics of the thin wire structures are displayed in Fig. 3.6. In contrary to the continuous wire structures [60] that exhibit a stopband with no lower edge, the present configuration exhibits a stopband with a well-defined lower edge due to the discontinuous nature of the wires.

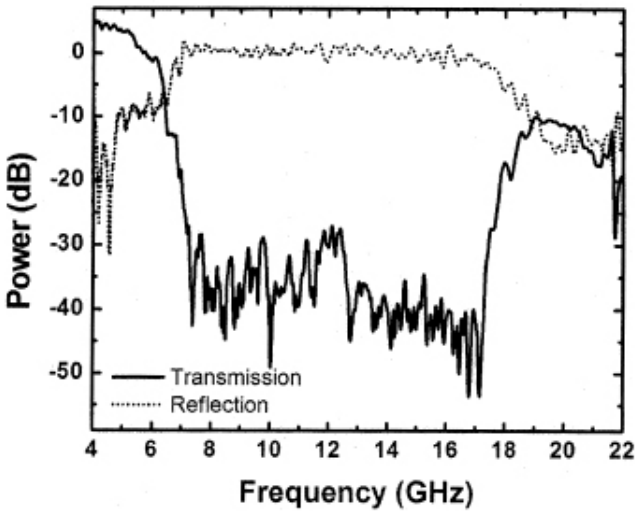

Fig. 3.6: Measured transmission and reflection spectra of the discontinuous thin wire medium.

The stopband of the discontinuous thin wire structure extends from 6 to 18 GHz. The transmission of the structure for the lower passband is higher than unity. This high transmission can be explained by the lensing effect and the spatial dispersive properties of our structure along with the experimental error due to the overall size of the crystal (which is around a few wavelengths at

these low frequencies). The transmission of the structure for the higher passband is measured to be less than - 10 dB. The reflection measurement indicates that all of the incident EM waves are reflected back from the structures within the stopband. So, the structure behaves like a good mirror throughout the stopband. For the passband region starting from 18 GHz, the measured reflection is near -15 dB. As the transmitted power is also low at these frequencies, we can conclude that the EM waves can not efficiently couple into propagating modes and strongly scatter within the structure.

At the frequency region 6-18 GHz, where no EM waves propagate inside the medium, periodic discontinuous wire structure has a negative effective dielectric permittivity, ε_{eff}. Effective magnetic permeability of the medium is equal to unity, since the structure do not contain any magnetic resonant elements that will respond to applied magnetic field.

3.3.2 Periodic "Split Ring Resonator" Medium

The negative permeability medium can be achieved by using an artificial material which is called split ring resonator (SRR) [5]. We constructed a periodical arrangement of copper SRRs on a circuit board to investigate the transmission and reflection characteristics of these exciting structures. A single copper SRR unit with parameters r_1 = 2.5 mm, r_2 = 3.6 mm, $d = w$ = 0.2 mm and t = 0.9 is shown in Fig. 3.7(a). It consists of two rings separated by a gap, which is similar to the SRR structures in [6]. Fig. 3.7(b) displays the stacked periodic SRR medium with number of unit cells in x, y and z directions N_x = 15, N_y = 15, and N_z = 20. The periodicity along x, y, and z axes are a_x = 8.8

mm, a_y = 8.8 mm, and a_z = 6.5 mm, respectively. Since we will later use SRR and wire media together to obtain a composite metamaterial, we choose the number of unit cells and periodicity of SRRs to be the same with the wire structures.

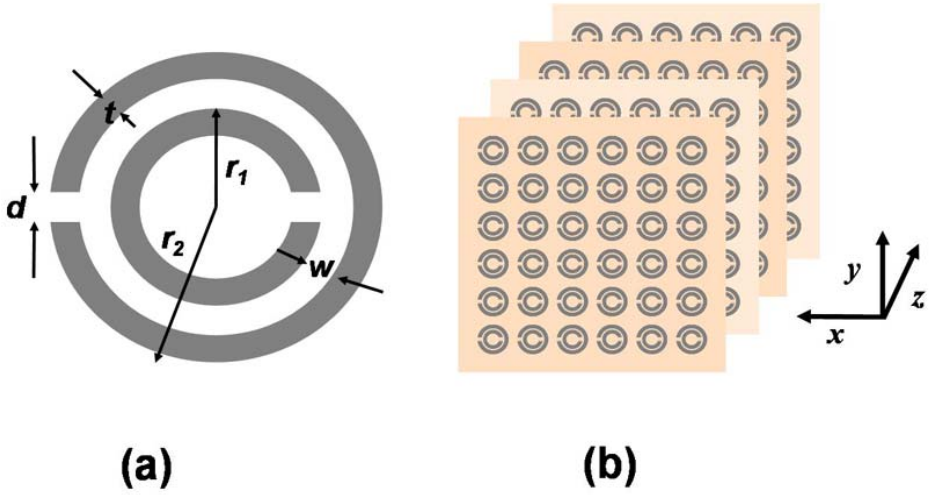

Fig. 3.7: Schematics of (a) single SRR unit, (b) periodical arrangement of SRRs

The measured transmission and reflection characteristics of the SRR medium are displayed in Fig. 3.8. The data shows that the structure has four significant pass bands, along with four stopbands throughout the spectrum. For the first passband, the transmission is measured to be higher than unity. As we have a passive structure with no gain, this high transmission effect can be explained by the lensing effect and crystal size restrictions as described in the previous section.

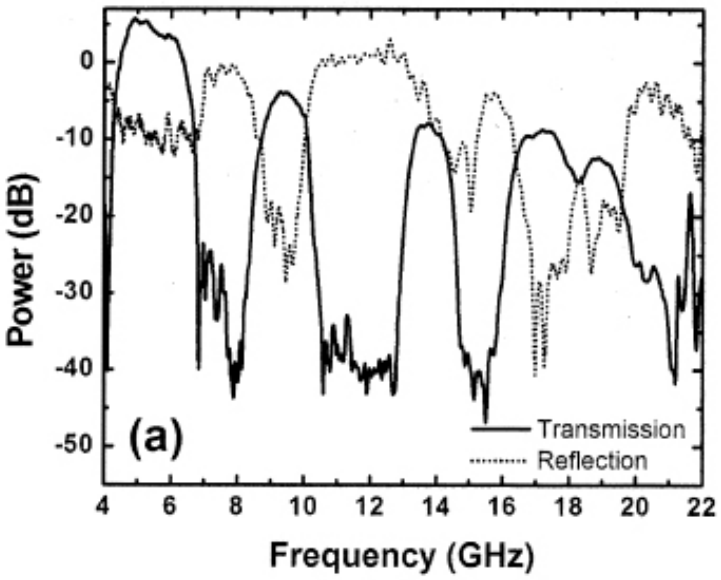

Fig. 3.8: Measured transmission and reflection spectra of the periodic split ring resonator medium.

The magnitude of transmission of the passbands decreases for the higher order passbands. While the second passband has a peak transmission of -5 dB, this reduces to -10 dB for the fourth passband. The measured reflections at the first and second stopbands are measured to be near unity. So, we can safely claim that these structures perfectly reflect the EM waves for the lower stopbands. However, the measured reflection for the higher stopbands is around -5 dB which is well below unity. This suggests that the EM waves are partially scattered within the structure at the higher stopbands.

The measured photon lifetime for the first passband, which is derived from phase measurements, is plotted in the Fig. 3.9. Photon lifetime corresponds to the propagation time of the EM waves inside the metamaterial [62]. Photon lifetime measurements will be a critical parameter in the following discussion,

since the group velocity is inversely proportional to the photon lifetime. As shown in the figure, the delay time significantly increases near the band edges.

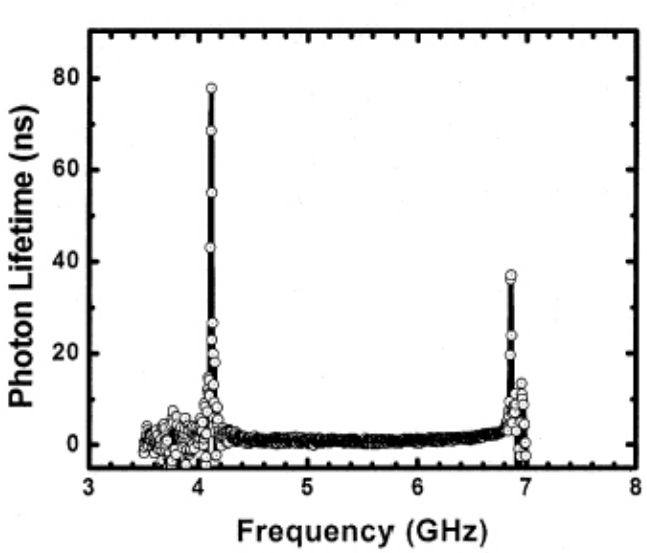

Fig. 3.9: Measured delay time, photon lifetime, as a function of frequency. The delay time increases rapidly as we approach the band edges.

The photon lifetime near the lower edge of the first passband is ~ 80 ns, which is 160 × larger than the time required for the EM waves to propagate along the structure. So, the SRR structure reduces the speed of light at this frequency by a factor of 160. For the upper edge, the lifetime is ~ 40 ns, which corresponds to an 80 × reduction for the speed of light.

3.3.3 Composite Metamaterial

The composite metamaterial structure is constructed by stacking the SRR and wire mediums periodically as shown in Fig. 3.10. The periodicity along the *z* direction is 6.5 mm, the same as in SRR and wire media.

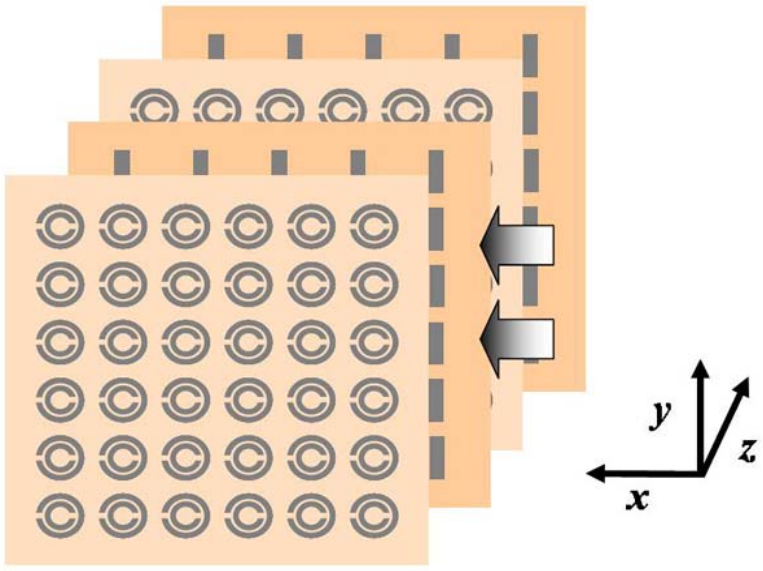

Fig 3.10: Schematic drawing of periodically arranged composite metamaterial composed of alternating layers of SRRs and wires.

The measured transmission and reflection properties of the composite metamaterial are displayed in Fig. 3.11. A broad passband extending from 9.6 to 14.3 GHz can be clearly seen there. The average transmission within the passband is around - 4.5 dB, corresponding to a transmission of -0.3 dB for each unit cell. As can be seen from Figs. 3.6 and 3.8, there is a frequency range (10 - 12.5 GHz) where a band gap is observed for both SRRs and wires. Since a transmission band covering this frequency range is observed for composite metamaterial, this can be taken as a possible left-handed property. But as we will discuss in the following chapter, this is not the case and this transmission band is indeed right-handed.

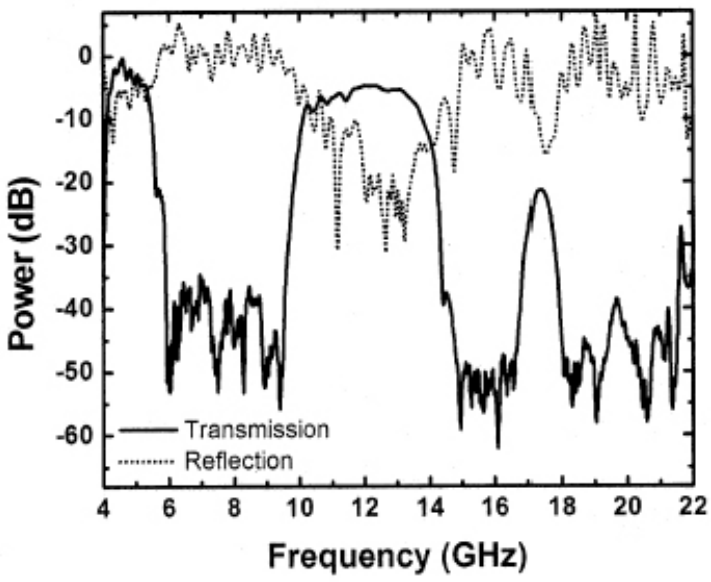

Fig 3.11: Measured transmission and reflection spectra of the composite metamaterial.

The reflection of the composite metamaterial structure within this frequency range is quite low. This shows that most of the EM waves penetrate into the composite medium, and we have a certain amount of scattering loss at these frequencies. The reflection of the structure is around unity for the first stopband region, which suggests that the composite structure acts as an almost perfect mirror for these frequencies.

3.4 Summary

In summary, we investigated the transmission and reflection properties of the composite metamaterials at microwave frequencies in free space. A transmission amplitude of -0.3 dB per unit cell is achieved throughout a

frequency range where a band gap is observed for both SRRs and wires. Moreover, we observed that the delay time increases very rapidly near the SRRs band edges.

Chapter 4

True Left-Handed Metamaterial

4.1 Introduction

In the previous chapter we investigated the transmission and reflection characteristics of SRR, discontinuous wire and composite metamaterial composed of SRR and wire structures. It is a well-known fact that the band gap observed for the wire medium is due to effective negative permittivity of the periodic structure. But it is not possible to say that the gaps observed (Fig. 3.8) for SRR structures are due to negative permeability. Since the SRR has a single magnetic resonance frequency, only one of the gaps could be due to negative permeability.

This chapter is organised as follows. First we identify the magnetic resonance and electric resonance of SRRs by using ring resonators with the splits closed. Then we verify the effect of interaction between SRRs and wires and experimentally demonstrate the shift in plasma frequency. We will investigate the effect of misalignment and periodicity to SRR's magnetic resonance gap. We will also provide a brief discussion about the difference of

transmission characteristics for continuous and discontinuous wire structures. Finally we will present a new CMM structure which exhibits true left-handed behavior and has a transmission band with a peak value of -1.2 dB, which is the highest transmission peak reported for a left-handed material.

4.2 Magnetic Resonance Gap of SRR Structure

4.2.1 Band gap formation analysis for SRR periodic structure

The split ring resonator has a large magnetic response against electromagnetic waves over certain frequencies. The magnetic resonance of SRR structure does not allow EM waves to propagate through a periodic medium composed of SRRs, hence a stop band occurs. SRR structures have also electric resonances [44,59] at certain frequencies where EM waves cannot propagate inside the medium due to negative effective permittivity. Hence, a bandgap in the transmission spectrum of periodic SRR medium may be due to the negative permittivity or the negative permeability or to the periodicity. The ambiguity can be removed by using a structure in which the splits in the ring resonators are closed (closed SRR). Closing the splits of ring resonator, will destroy the magnetic resonance but still keep the electric resonance. Therefore we expect to have a transmission band instead of a bandgap at frequencies of interest for negative magnetic permeability.

In the previous chapter we investigated the characteristics of the SRR structure shown in Fig. 3.7(a), where the splits in the rings are oriented at the left side of the outer ring, and the right side of the inner ring. Since the applied

electric field is at the *y* direction (Fig 3.7(a)), the discontinuities along the **E** field cause several band gaps at the transmission spectrum of periodic SRR medium (Fig. 3.8). So the SRR structures behave like a discontinuous wire and give a response to the applied electric field. That's the reason why we observed 4 band gaps between 4-22 GHz, in the previous chapter.

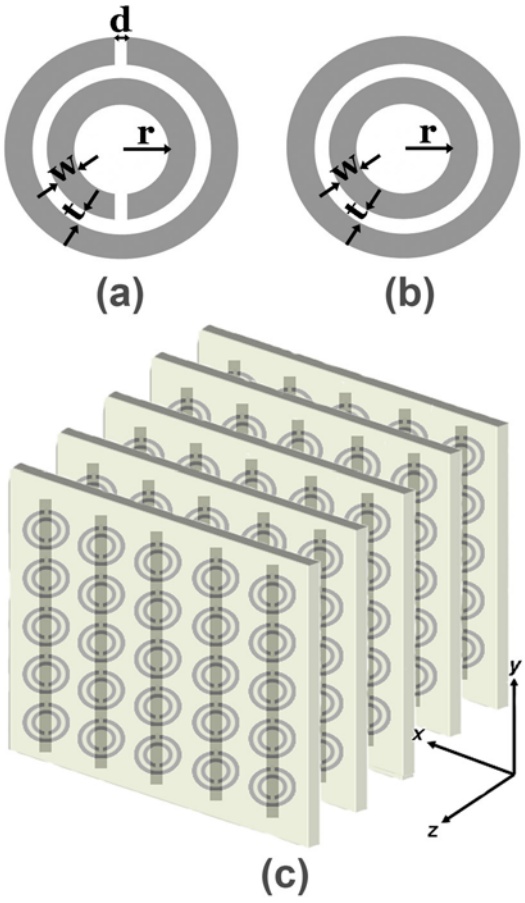

Fig. 4.1: Schematics of (a) a single split ring resonator (SRR) (b) a ring resonator with splits closed (CSRR) (c) Periodic CMM composed of SRRs on one side, wires on the other side of dielectric board.

Because of the discontinuity problem that was mentioned above, we switched to SRR structure shown in Fig. 4.1(a). In this case the splits in the rings are oriented at the top side of the outer ring, and the bottom side of the inner ring.

The parameters of the SRR are $d = t = 0.2$ mm, $w = 0.9$ mm and $r = 1.6$ mm. SRRs are arranged periodically with 5, 15, and 18 number of unit cells in the x, y and z directions respectively. Each unit cell contains a single SRR and the dimensions of the unit cell are $a_x = a_y = 8.8$ mm, and $a_z = 6.5$ mm. The experimental procedure is explained in the previous chapter (section 3.2.1).

Figure 4.2(a) shows the measured transmission spectra of periodic SRRs (solid line) and CSRRs (dashed line) between 3-14 GHz. The SRR medium displays two stop bands throughout the interested frequency range. The first band gap (3.55-4.05 GHz) of the SRR medium disappears for the CSRR medium (Fig 4.2(b)). We know that the reason for the magnetic resonance of SRRs is the splits in the rings. Hence, closing the splits will destroy the magnetic resonance of the SRR structure. This implies that this gap corresponds to the magnetic resonance gap of the SRR structure. Between 3.55-4.05 GHz electromagnetic waves cannot propagate inside the periodic SRR medium because effective magnetic permeability becomes negative. On the other hand, the second band gap (8.1-11.9 GHz) of the SRR medium essentially coincides with the stop band of the CSRR medium. Therefore the physical origin of this stop band can be attributed to the electric resonance of the periodic medium.

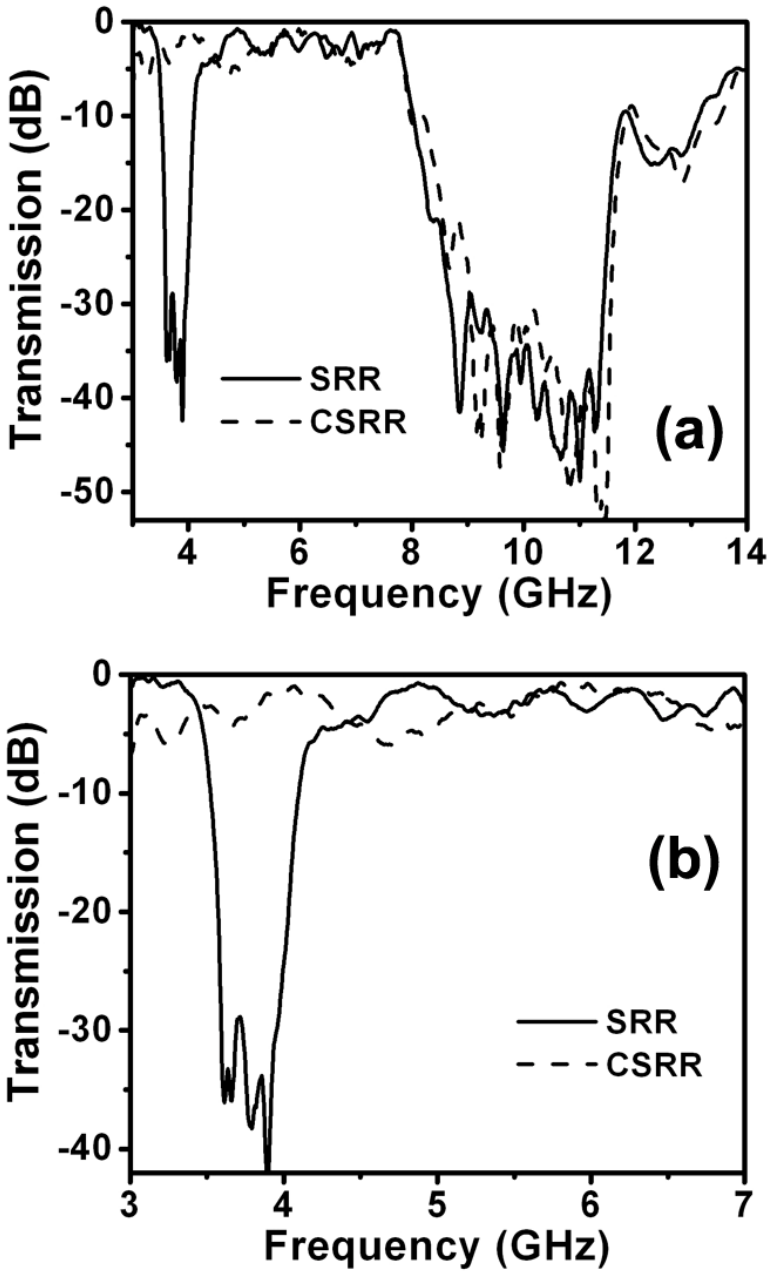

Fig 4.2: Measured transmission spectra of a periodic SRR medium (solid line) and periodic CSRR medium (dashed line) between (a) 3-14 GHz, (b) 3-7 GHz.

At the beginning, it was thought that the SRRs have effective permittivity equal to unity and they do not have any response to the applied electric field. This measurement clearly shows that the SRRs have also electric resonances similar to the discontinuous wire structures and stop bands of an SRR medium cannot be automatically assumed as "negative μ" behaviour. Some of the observed band gaps for SRRs could also be due to electrical response of the periodic SRR medium or Bragg gaps due to periodicity. If we turn back to the previous chapter, analyzing the transmission characteristics (Fig 3.8) under the light of these new findings the frequency range (10.5-12.5 GHz), where a band gap for SRR and transmission band for CMM occured, does not have negative permeability. Therefore that transmission peak cannot be called a left-handed transmission peak. But it is still an unusual transmission peak, and deserves interest, instead of naming the previous structure as a left-handed metamaterial, one can use another definition, namely "composite metamaterial".

4.2.2 Effect of Misalignment and Periodicity on the magnetic resonance gap

In a previous work published by Smith *et al.* [7], the misalignment problem is adressed. It is stated that the resonant frequency of the SRRs is *very* sensitive to small changes in parameters. This will be a huge problem if the slight misalignment affects the resonance frequency of the SRRs. Therefore, to understand the effect of misalignment in periodic SRR structures, we performed transmission measurements on misaligned SRR structures. Figure 4.3(a) depicts the measured transmission spectra of aligned (Fig. 4.3(b)) and slightly misaligned (Fig. 4.3(c)) SRR boards. We only misaligned the SRR structures along z direction, since the structures on the board are aligned in x

and *y* directions. As seen from Fig. 4.3(a) resonance gap of SRR remained same at the same frequency when SRR boards are slightly misaligned.

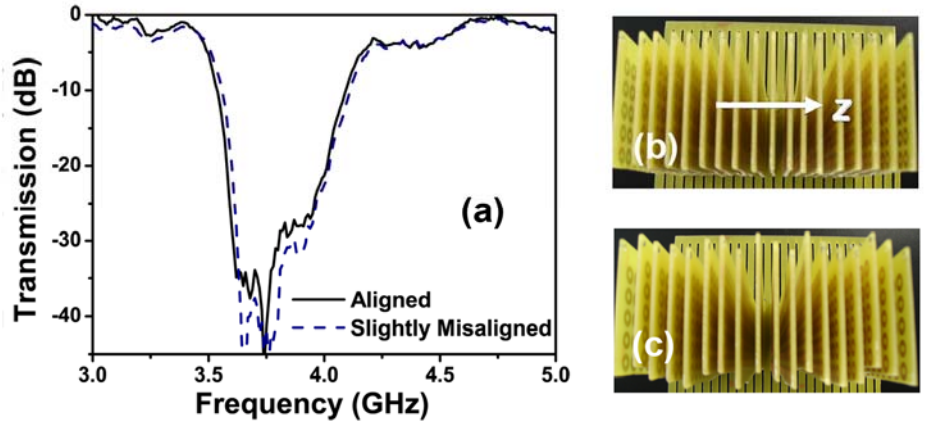

Fig. 4.3: (a) Measured transmission spectra of aligned (solid line) and slightly misaligned (dashed line) SRR structures. (b) Top view of aligned SRRs. (c) Top view of slightly misaligned SRRs.

We also checked an exaggerated case assuming that there is almost no alignment between boards in the *z* direction (Fig. 4.4(b)). Again the resonance gap of SRR did not disappear and the frequency region did not change even for a hardly misalignment SRR medium (Fig. 4.4(a)).

Another case is the effect of periodicity to the SRR resonance gap. By destroying the periodicity along *z* direction between SRR boards we obtained a non-periodic SRR medium as shown in Fig. 4.5(b). Transmission spectrum of non-periodic SRR structure is given in Fig. 4.5(a). The frequency range where SRRs have magnetic resonance still remains same even for non-periodic media.

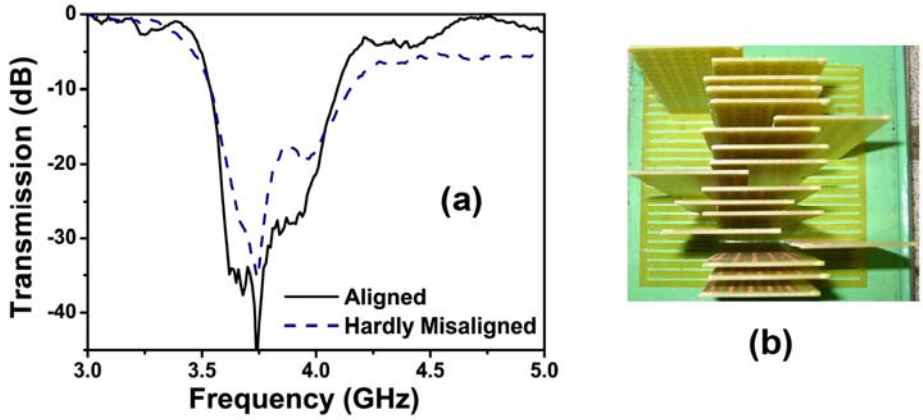

Fig. 4.4: (a) Measured transmission spectra of aligned and hardly misaligned SRR structures. (b) Top view of hardly misaligned SRRs.

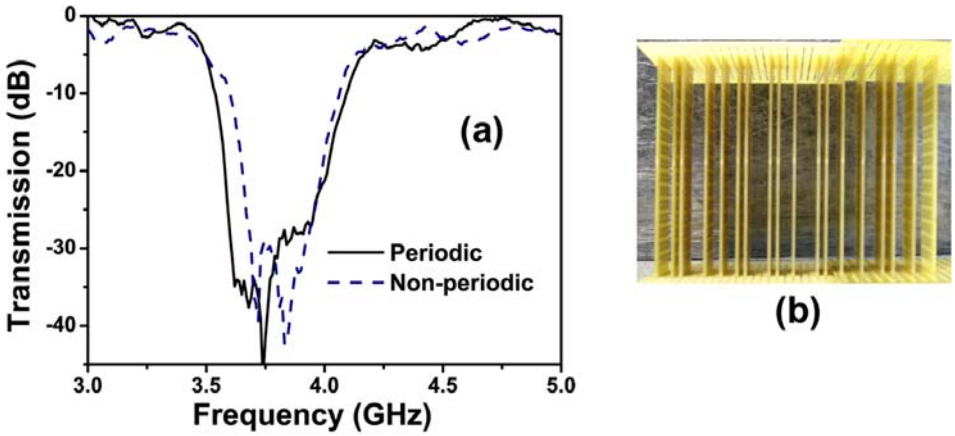

Fig. 4.5: (a) Measured transmission spectra of periodic (solid line) and non-periodic (dashed line) SRR structures. (b) Front view of non-periodic SRRs.

These measurements clearly show that misalignment is not a critical issue in the design of SRR structures, and the statement discussed by Smith *et al.* [7], is not the case in reality. Misaligning the SRR layers or destroying the periodicity does not affect the magnetic resonance gap and the resonance frequency of

SRR medium. Since each split ring resonator unit cell has a magnetic resonant frequency, having a bunch of SRR will still give a similar resonance gap obtained by periodic SRR medium. One may ask, why we bother with the periodic SRR structure if the periodicity is not important. The answer is, in order to construct a composite metamaterial we need a periodic SRR medium in order to group them with the wires. Periodicity is a critical issue for the wire case, because the plasma frequency of the wires strongly depends on the periodicity of the wire.

4.3 Electric responses

4.3.1 Comparison of continuous and discontinuous wire structures

In the third chapter, we investigated the transmission properties of discontinuous wire structures. As indicated in the previous section the magnetic resonance gap of SRRs is between 3.55 - 4.05 GHz, where effective permittivity for discontinuous wire medium is positive, since there is a transmission band at the indicated frequencies. However, for continuous wires the negative permittivity region extends from zero frequency to plasma frequency [60]. In the previous chapter, although we mentioned the difference between the discontinuous and continuous wire structures, we did not give experimental evidence.

The width and thicknesses of both wire structures are 0.9 mm and 30 μm, respectively. The periodicity along the *x*, *y*, and *z* axes are a_x = 8.8 mm, a_y =

8.8 mm, and a_z = 6.5 mm. The only difference is the discontunity introduced by a 0.35 mm gap for the case of discontinuous wire structures (Fig 3.5(a)). Figure 4.6 shows the measured transmission spectra of the continuous and discontinuous wires. As seen from the figure, the continuous wires have a plasma frequency around 8 GHz. Dielectric permittivity is negative below plasma frequency down to zero frequency, covering the resonance gap of the SRRs.

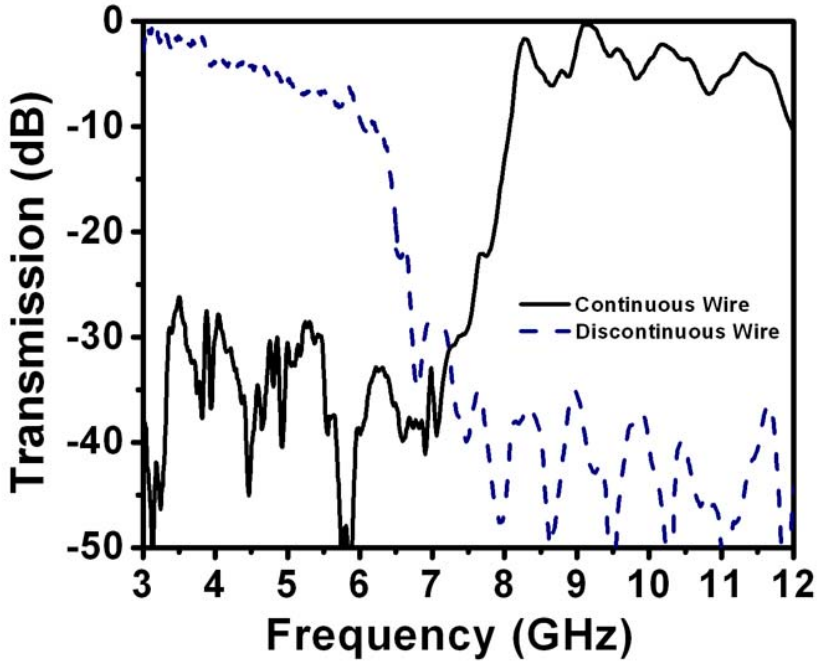

Fig. 4.6: Measured transmission spectra of continuous (solid line) and discontinuous wires (dashed line).

On the other hand for the discontinuous wires, there is a lower edge for the negative permittivity frequency range. The effective permittivity is negative

between 6-18 GHz, where 18 GHz is the plasma frequency for the periodic discontinuous wire material (Fig 3.6). So it would not be possible to construct a left-handed material using discontinuous wires since there is not a frequency range where both effective permittivity of wires and effective permeability of SRRs are negative. For this purpose, we will use continuous wires to construct a left-handed material.

4.3.2 Downward plasma frequency shift for CMM structures due to SRR's electric response

In this section, we will discuss the electric response of the CMM. Previously reported transmission results did not emphasize the interaction between SRR and wire structures. However, it was recently found [59] that the SRRs, in addition to their resonant magnetic response at ω_m, exhibit a resonant electric response at ω_0. This behavior is similar to the electric response of a system of cut-wires (wires of finite length) which exhibits a stop band with a well-defined lower edge due to the discontinuous nature of the wires. The SRR structures contribute to the effective permittivity of the CMM, causing a downward shift on the plasma frequency determined solely from wire structures. To demonstrate this effect, a CMM consisting of periodic alternating layers of CSRRs and wires is used. Thickness, length and the width of the wires are 30 μm, 13.5 cm and 0.9 mm respectively.

Figure 4.7 displays the measured transmission spectra of wire only (dashed line) and closed CMM (solid line) obtained by combining CSRR and wire. While the plasma frequency of the wire-only structure is around 8 GHz, the

plasma frequency is reduced down to 5.3 GHz for the closed CMM structure since both CSRRs and wires respond together to electric field. So the electric response of the CMM is the sum of the electric responses of the closed SRRs and the wires. As one can see from Fig. 4.7, the plasma frequency of the CCMM is much lower than that of the wires alone. Therefore it is important to determine whether the shift in plasma cut-off frequency covers the magnetic resonance gap, which would render the CMM as a right-handed medium. This effect must be taken into account in left-handed metamaterial designs.

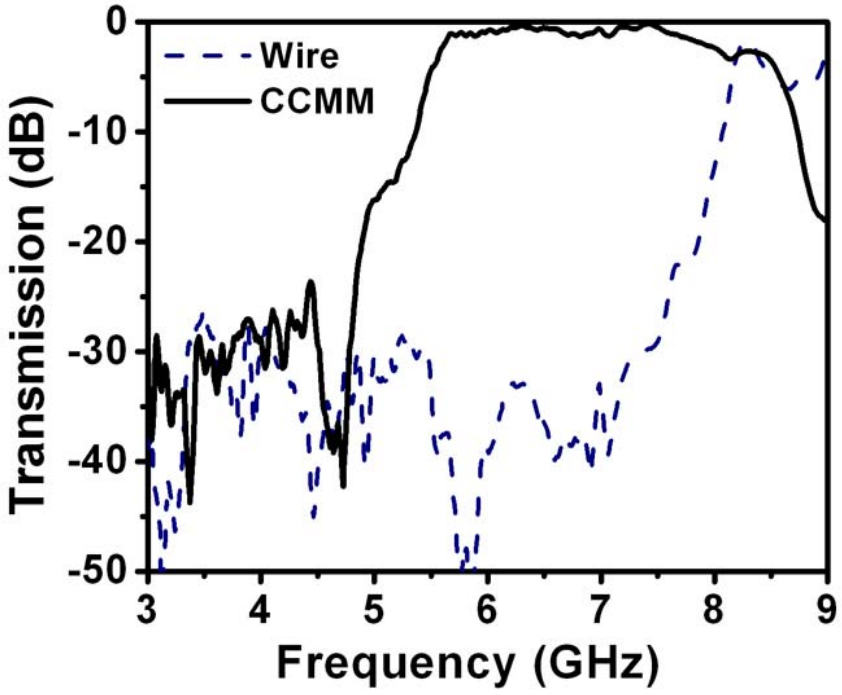

Fig. 4.7: Measured transmission spectra of wires (dashed line) and closed CMM (solid line) composed by arranging closed SRRs and wires periodically.

4.4 True Left-Handed Transmission Peak

We concentrate on the first band gap of SRR structure which is located between 3.55 - 4.05 GHz. We showed that this band gap is due to negative effective permeability of the medium, and we still have a negative effective permittivity after adding SRR into the wire medium.

The CMM structure is constructed by stacking the SRR and wire media periodically as shown in Fig. 4.1(c). We then measured the response of EM wave to the CMM structure, which is made of $N_x = 5$, $N_y = 15$, and $N_z = 24$ unit cells. Each unit cell has a single SRR, and a copper wire with lattice spacings of $a_x = a_y = 8.8$ mm, $a_z = 6.5$ mm. Measured transmission spectra for SRR only (solid line), wire only (dashed line) and CMM (bold solid line) periodic structures is displayed in Fig. 4.8.

As shown in Fig. 4.8, the SRR structure has a band gap (thus $\mu < 0$) between 3.55 and 4.05 GHz, and the wire structure has a band gap (thus $\varepsilon < 0$) up to 8 GHz. The CMM structure allows propagation of EM waves between 3.6 and 4.1 GHz, where both ε and μ are negative. The CMM pass band exactly coincides with the stop band of SRR. However, one has to know the plasma frequency ω_p of the combined system of SRRs and wires, and not only of the wires. As we have shown before in Fig. 4.7, ω_p for the combined system is much lower than the ω_p of the wires alone. Therefore, the transmission band is due to coupling of magnetic resonance of SRRs, and electric resonance of both wires and SRRs. The peak transmission amplitude at 3.9 GHz is -1.2 dB, which is a significantly high transmission value for a material made of metals.

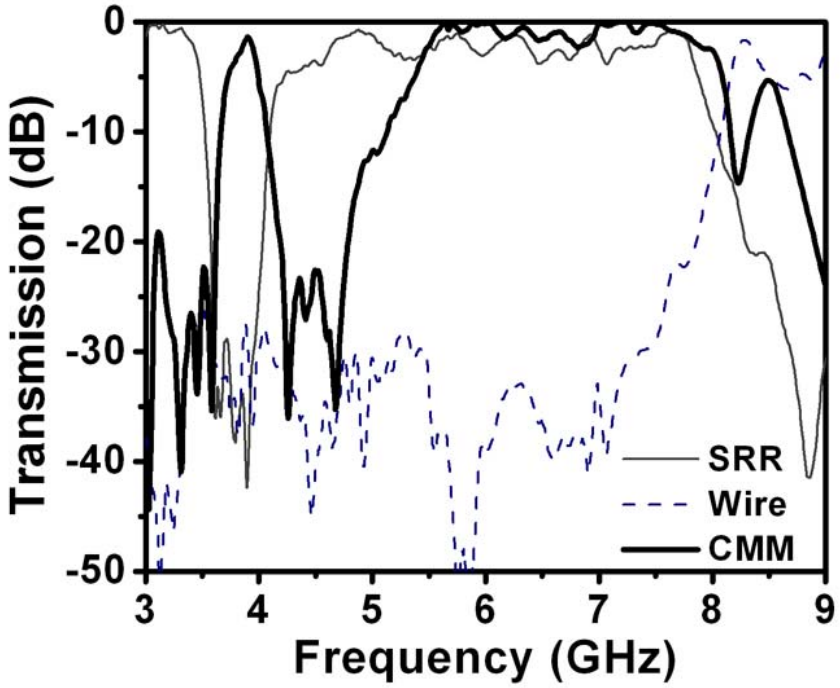

Fig 4.8: Measured transmission spectra of SRRs (solid line), wires (dashed line) and composite metamaterial (bold solid line).

Note that such a transmission band is not observed for closed CMM composed of CSRRs and wires (Fig. 4.7); therefore the transmission band is due to coupling of magnetic resonance of SRRs, and dielectric resonance of both wires and SRRs. Finally, if one uses the ω_p of the wires only (dashed line in Fig. 4.7 high transmission seen between 5.3 - 8 GHz can not be explained, since $\varepsilon < 0$ and $\mu > 0$. If $\varepsilon < 0$ for this frequency region, we expect to observe a gap instead of a pass band. This can be explained by Fig. 4.7, where the combined electric response of SRRs and wires results in $\varepsilon > 0$ for frequencies larger than 5.3 GHz. Therefore the electric response of both SRRs and wires

has to be taken into account in interpreting the CMM transmission experiments.

4.5 Summary

In conclusion, we have successfully demonstrated true left-handed behavior in free space with a high transmission peak. The left-handed transmission band exactly coincides with the region where both dielectric permittivity and magnetic permeability take negative values. By closing the splits of the SRRs, we experimentally verified the magnetic resonance of the SRR structures. By using this procedure the regions of negative permeability and negative permittivity of SRR structures can be successfully identified. We also confirmed experimentally that the ω_p of the CMM composed of SRRs and wires is lower than wires-only plasma frequency ω_p. We have also shown that misalignment and periodicity is not critical issues for resonance gap of SRRs. The difference between the dielectric responses for discontinuous and continuous wires is shown experimentally.

Chapter 5

Negative Refraction of 2D LHMs

5.1 Introduction

Left-handed materials have several unique physical properties, and the most exciting property of LHMs is negative refraction. Using left-handed materials one can change the way EM waves refract. Negative refraction is verified both theoretically [1,8] and experimentally [9]. After the negative refraction experiment by Smith *et al.*, an intense debate on negative refraction started. Valanju *et al.* claimed that dispersion implies positive refraction of group velocity even when the phase velocity is refracted negatively [10]. Also the effects of dispersion and loss on negative refraction experiments are criticized [11]. But further experimental studies on negative refraction, addressing the issues criticized, using different techniques supported the existence of negative refraction [13,14]. The concept of negative refraction has also been generalized to transmission-line structures. Negative refraction phenomena in microwave circuits were demonstrated by pursuing the analogy between circuit elements and material parameters [62].

Another characteristic of left-handed materials is that they support the propagation of plane waves with the phase velocity vector directed opposite to the Poynting vector. Such mediums can be described as negative phase velocity mediums, in contrast to conventional positive phase velocity mediums in which the phase velocity has the same direction as the power flow. Theoretical calculations and analyses issuing negative phase velocity mediums showed that phase velocity is negative in a left-handed material [63,64]. Also using a transmission-line model, phase velocity is shown to be negative both theoretically and experimentally [65]. To our knowledge experimental verification of negative phase velocity in left-handed materials has not been experimentally verified yet.

In this chapter, we will first investigate the transmission characteristics of 2D LHMs. Then, the refraction spectra of a 2D CMM wedge structure will be shown, which clearly exhibits negative refraction behavior. Later, we will present direct experimental evidence that the phase velocity is negative within the left-handed pass band of a CMM. To contrast this, we will also show that the phase velocity is positive within another pass band of the CMM, where it is known to act as a right-handed medium. We have found very good agreement between the values of negative index of refraction obtained from phase spectra and from the refraction data, by employing Snell's Law.

5.2 Transmission Through 2D LHM

In the previous chapters we reported the transmission characteristics of 1D composite metamaterials, in which we have observed a true left-handed transmission peak. Left-handed properties of 1D LHM structures are restricted

to one dimension. Any experiment validating the anticipated reversals of electromagnetic properties requires at least 2D isotropy, in order to exhibit a left-handed characteristic for any angle of incidence. 1D structures are anisotropic compared to 2D structures and for some applications this anisotropic behavior may be undesirable. For example to verify negative refraction, EM waves are sent to the surface with an incident angle different than zero. 1D structures will respond to the EM wave only in one direction, therefore, only the component of the wave vector along that direction will be negatively refracted. But for the 2D case we have a negative refraction for both components of the wave-vectors. To achieve the highest isotropy 3D LHMs can be used but it is difficult to design a 3D medium that will respond to an incident field in all directions using the current designs.

To verify whether the 2D LHM has a negative refractive index or not, one has to be sure of whether 2D LHM has a left-handed transmission band similar to 1D structures, or not. For this purpose we investigated the transmission characteristics of 2D LHMs by using the same method as in the 1D case.

The SRR and wire patterns are fabricated on the front and back sides of the FR4 circuit boards respectively, with a copper deposited layer of thickness 30 μm. The geometrical parameters of the SRR and wire elements can be found in the previous chapter [pg. 42]. The unit cell consists of two SRRs and two wires in *x*-*z* planes, as shown in shaded parts of Fig. 5.1. The 2D CMM structure is made of $N_x = 5$, $N_y = 20$, and $N_z = 40$ unit cells, with lattice spacings $a_x = a_y = a_z = 9.3$ mm. The transmission experiment procedure is same with the 1D case as discussed in detail in chapter 3.

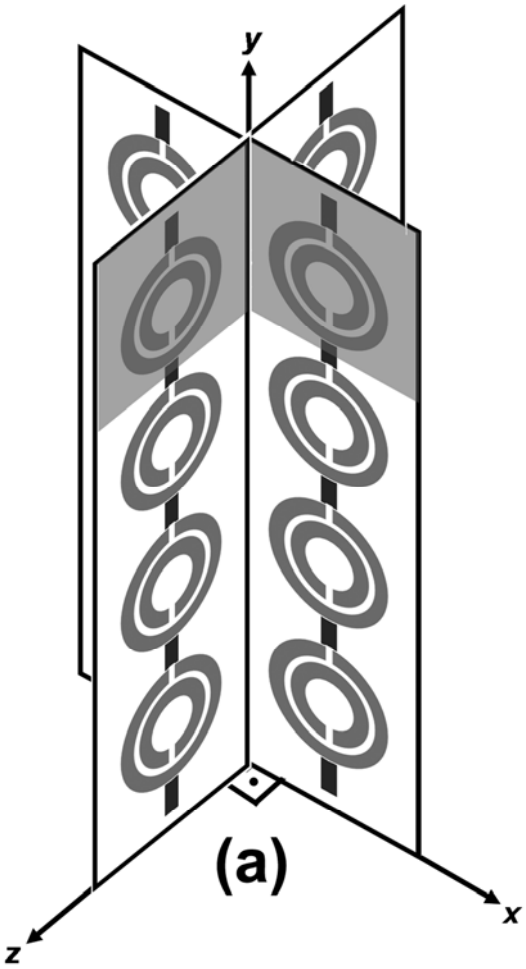

Fig. 5.1: Schematic drawing of 2D CMM structure. Shaded area shows the unit cell of the structure.

Figure 5.2 shows the measured transmission spectra of periodic SRRs, wires and 2D CMM between 3-7 GHz. The band gap of SRR between 3.55-4.05 GHz is due to magnetic resonance of periodic SRR medium, hence $\mu(\omega) < 0$ for this frequency range. The 2D CMM structure allows propagation of EM waves between 3.7 and 4.1 GHz, where both ε and μ are negative. The CMM pass band coincides exactly with the stop band of SRR. The transmission peak at

3.92 GHz is -10.2 dB, which is a significantly higher than the previously reported 2D CMM structures [7,13]

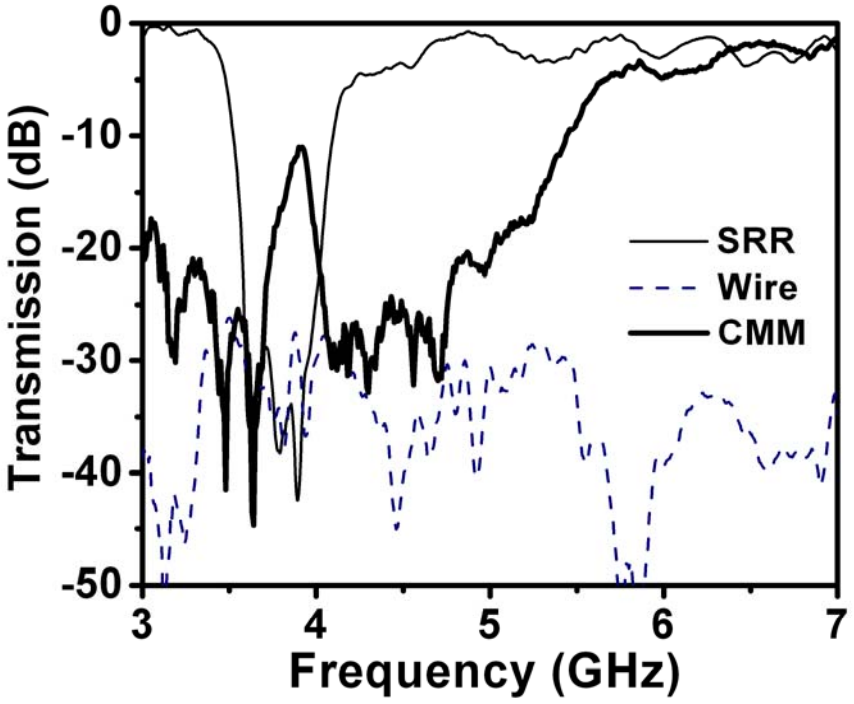

Fig 5.2. Measured transmission spectra of a periodic SRR medium (solid line) and periodic CSRR medium (dashed line) between (a) 3-14 GHz, (b) 3-7 GHz.

Compared to 1D CMM transmission peak values of -1.2 dB reported in chapter 4, the main contribution to the increased loss comes from the metal on the boards that are perpendicular to the propagation direction. We stress that the increase in loss is inherent to the dimensionality of the structure. The transmission band starting from 5.3 GHz is due to downward plasma frequency

shift, since the $\varepsilon > 0$ regime of the combined electric response of SRRs and wires starts at 5.3 GHz.

5.3 Negative Refraction in 2D LHMs

Negative refraction in 1D [14] and 2D [9,13] LHMs are shown experimentally by various groups. Two similar experiments [9,13] are performed in a waveguide chamber, with same test structures where the losses in the structures are high and the height of sample is limited to a three unit cell. The other experiment [14] is performed using a microwave lens to focus the incident beam, which would render the plane wave property. In our experiments we have samples that have shown high transmission and a height that is 20 times larger. We performed the negative refraction experiments in free space without using lenses, since using a microwave lens is nonsense. Therefore, our experimental method does not have the indicated problems of previous negative refraction experiments, and shows exactly that the EM waves are refracted negatively at the left-handed frequency region of the composite metamaterial.

5.3.1 Negative Refraction Experimental Setup

In our experiments we used a prism-shaped (wedge) structure composed of 2D left-handed material. If we transmit EM waves to the first interface of the wedge sample as shown in Fig. 5.3, the incident beam will not be refracted at this surface, since it enters into the wedge sample with an incident angle of 90° degrees. The refraction will occur in the second interface of the wedge sample

where the incident beam that is inside approaches the normal of the sample with an angle equal to the wedge angle. If the wedge sample has a positive refractive index, the beam will be refracted at the left side of the normal. However, if the wedge structure is constructed with a negative index material, refraction will occur at the other side of the normal corresponding to the right side of the normal in Fig. 5.3.

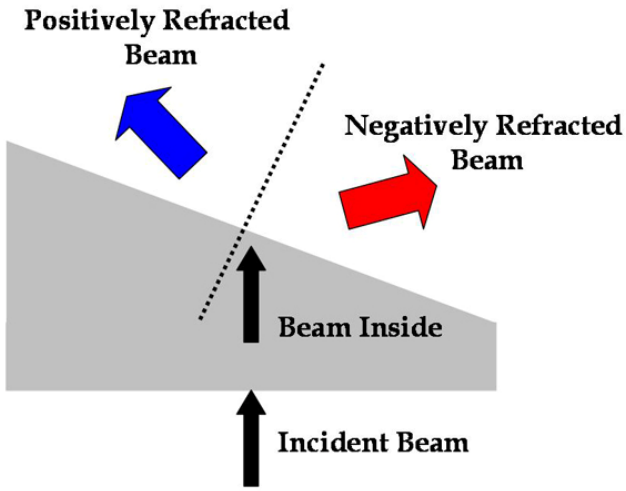

Fig. 5.3: Schematic drawing of refraction of incident beam passing from a wedge sample to air. Both positive and negative refraction cases are sketched.

Using the idea discussed above we constructed an experimental setup which is schematically drawn in Fig. 5.4. Two horn antennas are used in our experiments. The advantage of using a horn antenna instead of a waveguide as in previous refraction experiments [9,14] ensures that a true plane wave is transmitted to the first interface. To achieve a better resolution we used a horn antenna as a receiver. The source is located 13 cm (~2λ) away from the first interface of the wedge. The receiver antenna is mounted on a rotating arm to

obtain the angular distribution of the transmitted signal. The receiver antenna is located at a distance of 70 cm (~10λ) away from the second interface of the wedge. We measured the transmission in free space without the wedge sample in between, and used this data as a calibration. Then we inserted the sample and measured the transmission by rotating the receiver antenna with 2.5° steps.

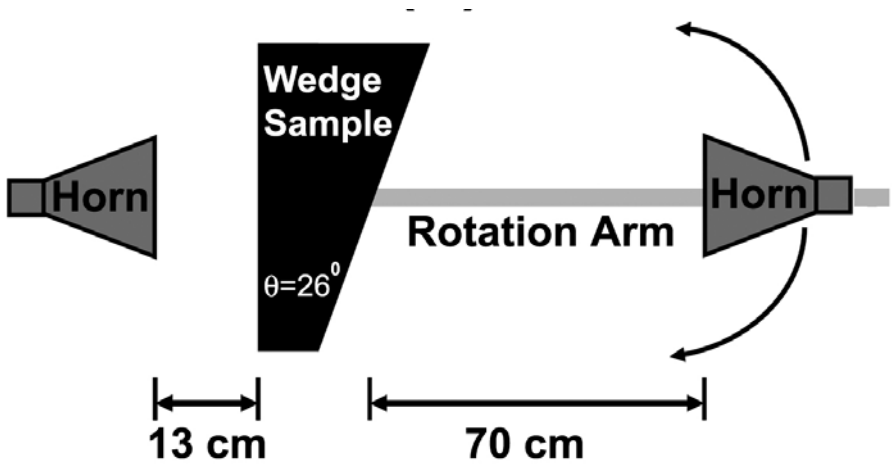

Fig. 5.4: Schematic drawing of experimental setup used for negative refraction experiment.

A wedge structure is constructed to test the negative refraction of 2D LHMs by cutting the boards and assembling them as shown in Fig. 5.5. Lattice spacings of the wedge are $a_x = a_y = a_z = 9.3$ mm. The minimum and maximum number of unit cells at the propagation direction is 3 and 19, respectively. So the average number of layers, also corresponding to the number of layers at the center of the wedge is 11 layers. 2 consecutive layers along the x direction have the same number of layers along z direction. Then the number of layers along the z direction is reduced by one. By using this two by one design, we obtained a wedge angle of $\theta = 26°$.

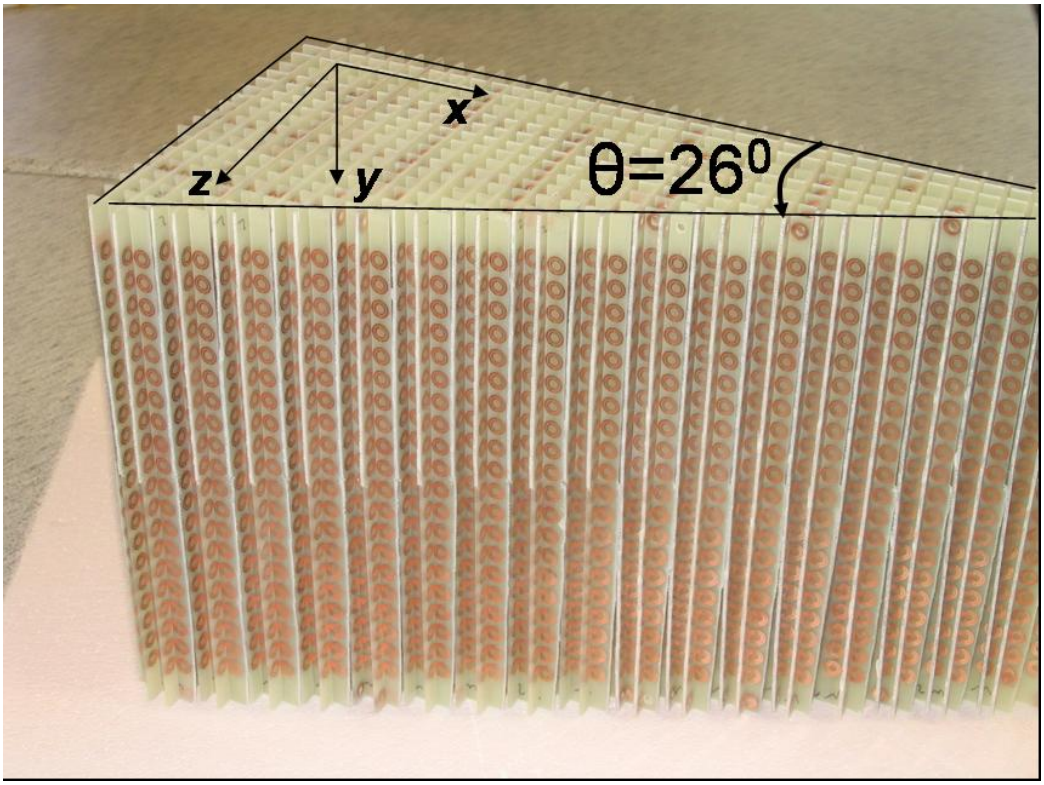

Fig. 5.5: 2D wedge structure.

5.3.2 Experimental Verification of Negative Refraction

The angular refraction spectrum is scanned by $\Delta\theta = 2.5°$ steps, while the frequency is swept from 3.73 GHz to 4.05 GHz in 400 steps, averaged over 256 measurements at each frequency. Figure 5.6 displays the intensity spectrum as a function of frequency and refraction angle. It is evident from the figure that the transmitted beam is refracted on the negative side of the normal.

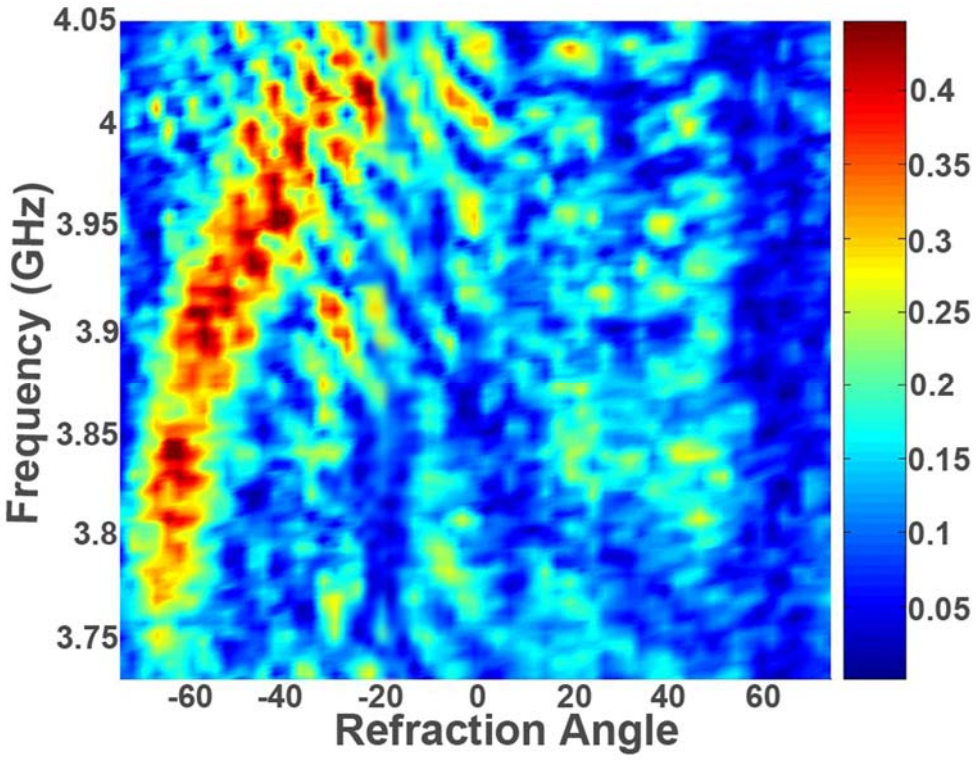

Fig. 5.6: Measured intensity spectrum of wedge shaped LHM sample as a function of frequency and refraction angle

Transmission characteristics of 2D LHM (Fig. 5.2) showed that there is a left-handed transmission band between 3.73 - 4.05 GHz. As seen from Fig. 5.6, the incident beam is refracted with negative refraction angles at the relevant frequencies. Previous experiments [9,13,14] have shown a negative refraction at a single frequency, such an analysis of a broad frequency range have not been done yet. If Fig 5.6 is analyzed in detail, it is clearly seen that refraction angle values, therefore negative refractive indices are not the same in all frequencies. At lower frequencies the EM waves are refracted at higher negative refraction angles, which results in a higher negative refractive index. The refraction index is lowered if we go to higher frequencies. This kind of

behavior is predicted theoretically [13], therefore our experimental results confirm the theoretical analysis.

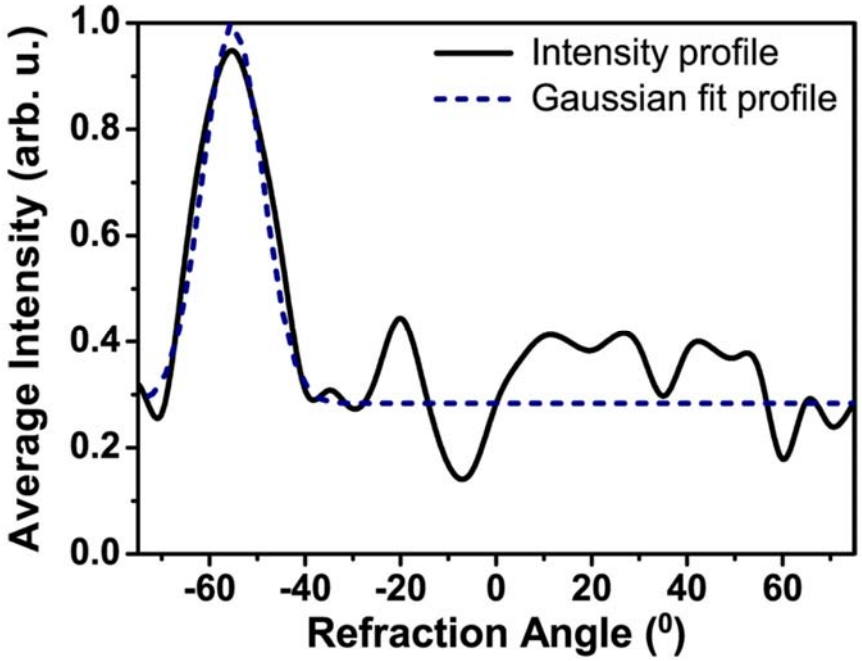

Fig. 5.7: The angular cross section of transmitted beam at 3.92 GHz.

To investigate the refracted beam profile, the angular cross section at a single frequency, f = 3.92 GHz is plotted in Fig. 5.7. We note that the incident field has a Gaussian beam profile centered at x = 0 (not shown on figure). The intensity of the transmitted beam is normalized with respect to the maximum. By applying a Gaussian profile fit to the lateral intensity distribution and by employing Snell's law ($n_{CMM}\sin\theta_i = n_{air}\sin\theta_r$) an effective refractive index can be defined for the CMM. For θ_i = 26°, EM wave is refracted at an angle of θ_r = 55°, from Snell's law we obtain n_{eff} = -1.87 ± 0.05 at 3.92 GHz.

5.4 Negative Phase Velocity

5.4.1 Experimental Verification of Negative Phase Velocity

Phase velocity is given by $v_{ph} = c/n$, where c is the velocity of light in vacuum and n is the refractive index of the medium. Since c is positive, a negative refractive index implies that phase velocity is negative. Negative phase velocity can be verified by measuring the phase shift of CMMs between different lengths at the propagation direction.

To demonstrate the negative phase velocity, we measured the transmitted phase of CMMs between 3-7 GHz. We measured the transmission phase in air, and used this data as calibration. Phase measurements are performed on rectangular slabs of CMMs. Reducing the number of layers by one decreases the length of the samples along propagation direction. We performed experiments for 5 different numbers of layers varying from 5 to 9. HP 8510 C network analyzer measures the transmitted phase within $[-\pi, \pi]$ range therefore measured phase data is unwrapped to obtain the phase profile. Figure 5.8 shows the transmitted phase of the CMMs between 5.4 - 7 GHz. As shown in the figure, when the length of the CMM is increased, phase also increases, which is a typical right-handed behavior. We have shown that at this frequency region ε_{eff} and μ_{eff} are both positive (Fig. 5.2). Therefore CMM exhibits right-handed characteristics between 5.4 - 7 GHz.

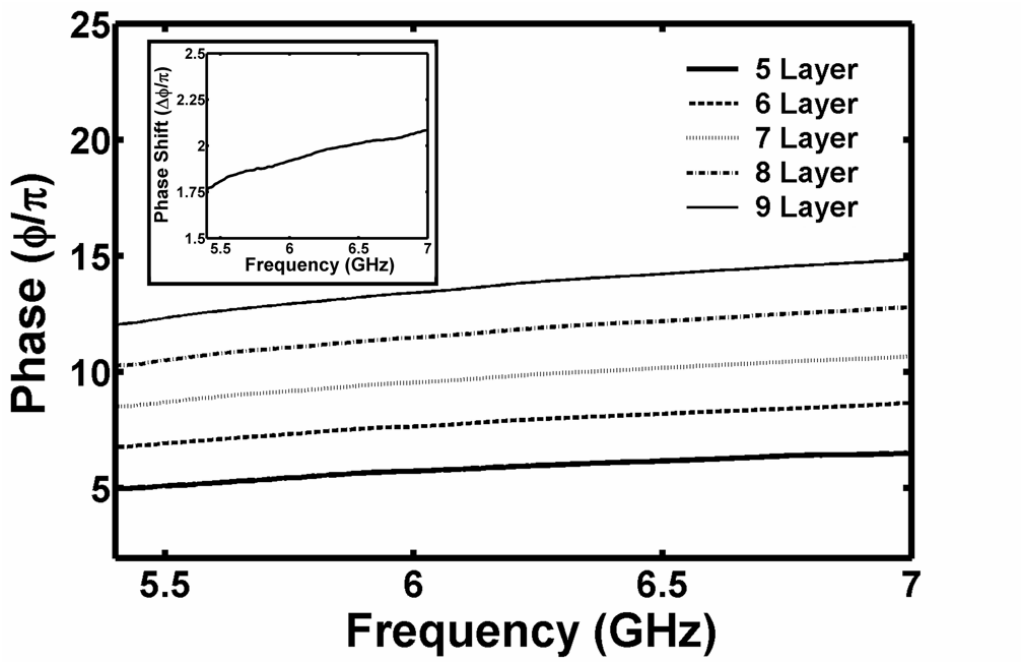

Fig. 5.8: Unwrapped transmission phase data obtained from different lengths of CMM between 5.4 - 7.0 GHz, where right-handed transmission peak takes place. Inset: Average phase difference between consecutive numbers of layers of CMM. Phase shift is positive between 5.4 - 7.0 GHz.

On the other hand, for the left-handed frequency region we observed a different behavior. The transmitted phase of the CMMs between 3.73 - 4.05 GHz is displayed in Fig. 5.9. As is clearly seen in the figure, increasing the length of the sample decreases the transmitted phase, a characteristic behavior for negative refractive index materials. This measurement clearly indicates that the behavior of phase is entirely different in left-handed materials, and the phase advances negatively in LHMs. Therefore, we can conclude that phase velocity possesses negative values inside LHMs.

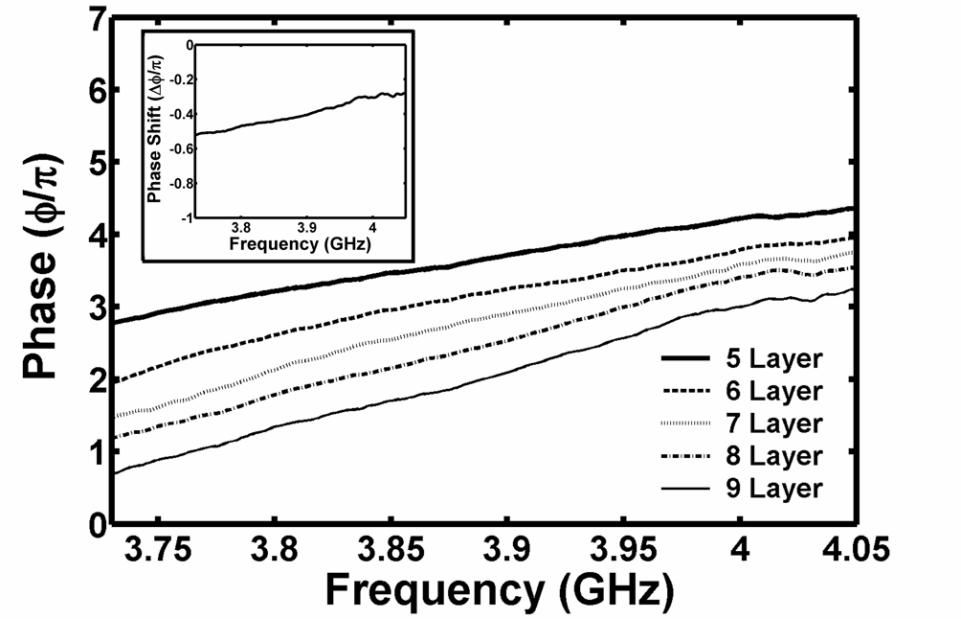

Fig. 5.9: Unwrapped transmission phase data obtained from different lengths of CMM between 3.73 - 4.05 GHz, where left-handed transmission peak takes place. Inset: Average phase difference between consecutive numbers of layers of CMM. Phase shift is negative between 3.73 - 4.05 GHz.

5.4.2 Index of Refraction Calculation from Phase Shift

In the previous section we discussed the transmission phase characteristics of CMMs with different number of layers along the propagation direction. In this section we will consider the phase shift of CMMs. Transmission phases of consecutive number of layers are subtracted, and phase shifts are averaged.

The average phase shifts between consecutive numbers of layers of CMM at the frequency ranges where CMM exhibits left-handed (3.73 - 4.05 GHz) and right-handed (5.4 - 7 GHz) characteristics are depicted in (inset of Fig. 5.9) and

(inset of Fig. 5.8), respectively. Phase shift for the frequency range where $n > 0$, is found to be positive as usual. Expectedly, phase shift is negative for the left-handed frequency range, which indicates that the phase velocity is negative

One can find the value of a refractive index by using the phase shift between consecutive numbers of layers of CMM. Phase velocity is defined as

$$v_{ph} = \frac{c}{n} = \frac{\omega}{k} \tag{5.1}$$

Then using (5.1), the refraction index can be defined in terms of a wavevector, speed of light and frequency as

$$n = \frac{ck}{\omega} \tag{5.2}$$

where k is simply

$$k = \frac{\Delta\phi}{\Delta L} \tag{5.3}$$

If (5.3) is inserted in (5.2) we obtain the final formula for the refractive index as

$$n = \frac{\Delta\phi.c}{\omega.\Delta L} \tag{5.4}$$

At f = 3.92 GHz, the average phase shift between consecutive CMM layers is measured to be $\Delta\Phi$ = -0.41 ± 0.05 π. If we insert these parameters into (5.4), the effective refractive index is found to be n_{eff} = -1.78 ± 0.22, which is close to the value -1.87 ± 0.05 obtained from the refraction experiment. The measured phase velocity at 3.92 GHz is negative and equal to -0.51c. At f = 3.98 GHz n_{eff} obtained from the refraction experiment is found as n = -2.02 ± 0.05, while the

value obtained from the phase shift is n = -1.97 ± 0.22. Also at f = 3.84 GHz, the values obtained from the refraction experiment (n = -1.22 ± 0.05), and the phase shift experiment (n = -1.28 ± 0.21) are in good agreement. Fig. 5.10 displays the values of negative refractive indices obtained from the refraction experiments and the phase measurements. There is a quite good agreement between these two experimental results.

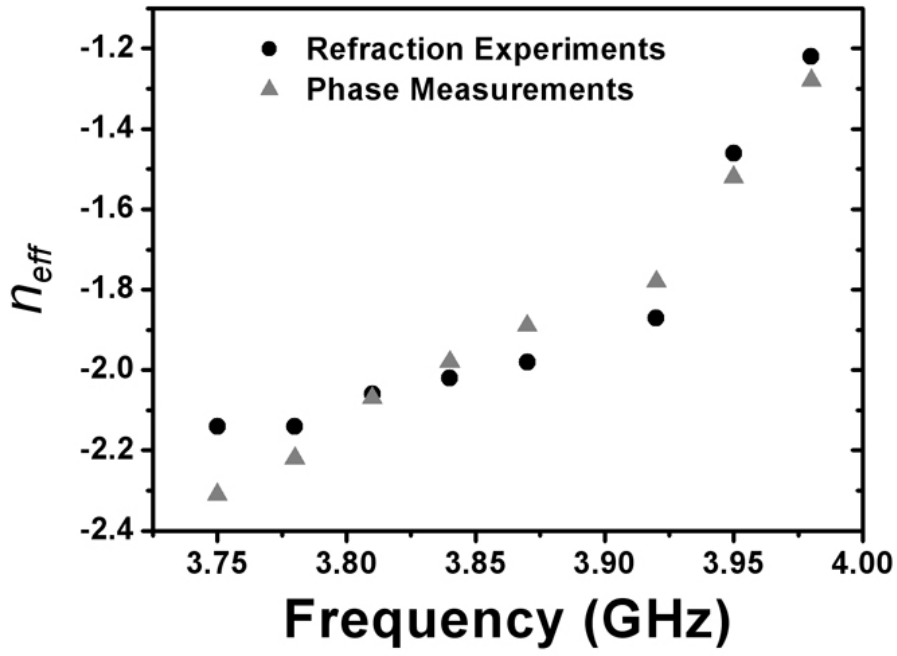

Fig. 5.10: The values of negative refractive indices obtained by using two experimental methods; the refraction experiments and the phase shift measurements. There is a quite good agreement for the values of negative refractive indices for these two experimental methods.

5.5 Summary

In conclusion, we have successfully demonstrated negative true left-handed behavior for 2D CMMs in free space with a high transmission peak. We also showed that CMM refracts the wave negatively where both permittivity and permeability posses negative values. Phase velocity is shown to be negative, and the values of the refractive indices obtained from the refraction experiment and the phase shift experiment are in good agreement.

Chapter 6

Conclusion and Future Directions

This chapter includes a brief summary of previous chapters and the results of this thesis work. In addition, we will briefly mention the new questions and possible future work that our results have led us to.

In the second chapter, we had a detailed discussion about the theoretical background of left-handed materials. We provided theoretical information about the components of a left-handed material, negative permittivity and negative permeability structures. We also showed that the simultaneous negative values for permittivity and permeability results in negative refraction.

In the third chapter, we investigated the transmission and reflection characteristics of a composite metamaterial (CMM). The CMM has an unusual transmission band at a frequency where SRR-only and wire-only structures have a band gap. In the fourth chapter, we obtained a true left-handed transmission peak, with a peak value of -1.2 dB. This is the highest transmission peak reported for a left-handed metamaterial. The magnetic resonance and electric resonance of SRRs are clearly distinguished by using

ring resonators with the splits closed. We then verified the effect of the interaction between SRRs and wires and demonstrate experimentally the downward shift in plasma frequency.

In the fifth chapter, we experimentally demonstrated a negative refractive index for 2D LHM at the frequencies where a left-handed transmission peak occurred. Moreover, we presented direct experimental evidence that the phase velocity is negative within the left-handed pass band of a CMM. The refractive index values obtained from the refraction experiment (-1.87) and calculated by using the phase shift between the layers (-1.78) are in good agreement.

Since the study of left–handed materials is a hot topic in the scientific community, there are several discussions questioning the problems of the left-handed materials. Using a metal-based left-handed material will cause higher losses and absorptions at higher frequencies, which is not particle and desirable. For technical applications, composite metamaterials must be scaled down, to achieve left-handed behavior at higher frequencies. We will search for the possibilities of scaling down the left-handed materials. For this purpose, we started the fabrication of metamaterials working around 100 GHz, in which the characterization is left for future work.

One of the interesting applications of LHMs is a perfect lens and focusing by a slab. Since we verified that our structures have a negative refractive index, we will try to construct a slab lens made of LHM that focuses EM waves. Another possible research topic is to match the impedance of LHM to achieve higher transmission, since reflection will not occur at the interface. LHM have both positive and negative indices throughout the frequency spectrum,

therefore around the crossover point ($n = 0$), a highly directive antenna can be obtained. Finally by adding active elements such as ferroelectric and ferromagnetic materials, we will try to tune the left-handed metamaterials.

List of Publications

[1] Mehmet Bayindir, K. Aydin, E. Ozbay, P. Markos and C. M. Soukoulis, "Transmission properties of composite metamaterials in free space," *Appl. Phys. Lett.*, vol. 81, p. 120, 2002.

[2] Ekmel Ozbay, Koray Aydin, Ertugrul Cubukcu, Mehmet Bayindir, "Transmission and Reflection Properties of Composite Double Negative Metamaterials in Free Space," *IEEE Trans. Antennas Propag.*, vol. 51, p. 2592, 2003.

[3] Koray Aydin, Kaan Guven, L. Zhang, M. Kafesaki, C. M. Soukoulis, and Ekmel Ozbay, "Experimental Observation of True Left-handed Transmission Peak in Metamaterials," *To be published in Opt. Lett.*, 2004.

[4] Koray Aydin, Kaan Guven, and Ekmel Ozbay, "Observation of Negative Refraction and Negative Phase Velocity in Left-Handed Metamaterials", *Submitted to Appl. Phys. Lett.*, 2004.

In addition to left-handed metamaterials, research was also carried out on 2D photonic crystals. Negative refraction and subwavelength resolution is achieved and these achievements resulted in an additional number of SCI journal publications.

[5] Ertugrul Cubukcu, Koray Aydin, Ekmel Ozbay, S. Foteinopoulou, and Costas M. Soukoulis, “Electromagnetic waves: Negative refraction by photonic crystals,” *Nature*, vol. 423, p. 604, 2003.

[6] E. Cubukcu, K. Aydin, S. Foteinopolou, C. M. Soukoulis, and E. Ozbay, “Subwavelength Resolution in a Two-Dimensional Photonic Crystal Based Superlens,” *Phys. Rev. Lett.*, vol. 91, p. 207401, 2003.

[7] Kaan Guven, Koray Aydin, K. B. Alici, C. M. Soukoulis, and Ekmel Ozbay, “Spectral negative refraction and point focusing analysis of a two-dimensional left-handed photonic crystal lens,” *Submitted to Phys. Rev. B*, 2004.

[8] Ekmel Ozbay, Kaan Guven, Koray Aydin, and Mehmet Bayindir, “Physics and Applications of Photonic Nanocrystals,” *To be published in International Journal of Nanotechnology*, 2004.

[9] K. Guven, I. Bulu, K. Aydin, H. Caglayan, and E. Ozbay, “Physics and Applications of Photonic Crystals,” *To be published in Photonic and Nanostructures – Fundamental Applications*, 2004.

Bibliography

[1] V. G. Veselago, “The electrodynamics of substances with simultaneously negative values of permittivity and permeability,” *Sov. Phys. USPEKHI*, vol. 10, p. 509, 1968.

[2] J. B. Pendry, A. J. Holden, W. J. Stewart and I. Youngs, “Extremely Low Frequency Plasmons in Metallic Mesostructures,” *Phys. Rev. Lett.*, vol. 76, p. 4773, 1996.

[3] J. B. Pendry, A. J. Holden, D. J. Robbins, and W. J. Stewart, “Low frequency plasmons in thin-wire structures,” *Journal of Physics: Condensed Matter*, vol. 10, p. 4785, 1998.

[4] D. R. Smith, D. C. Vier, Willie Padilla, Syrus C. Nemat-Nasser, and S. Schultz, “Loop-wire medium for investigating plasmons at microwave frequencies,” *Appl. Phys. Lett.*, vol. 75, p. 1425, 1999.

[5] J. B. Pendry, A. J. Holden, D. J. Robbins, and W. J. Stewart, “Magnetism from conductors and enhanced nonlinear phenomena,” *IEEE Trans. Microwave Theory Tech.*, vol. 47, p. 2075, 1999.

[6] D. R. Smith, Willie J. Padilla, D. C. Vier, S. C. Nemat-Nasser, and S. Schultz, “Composite medium with simultaneously negative permeability and permittivity,” *Phys. Rev. Lett.*, vol. 84, p. 4184, 2000.

[7] R. A. Shelby, D. R. Smith, S. C. Nemat-Nasser, and S. Schultz, “Microwave transmission through a two-dimensional, isotropic, left-handed metamaterial,” *Appl. Phys. Lett.*, vol. 78, p. 489, 2001.

[8] D. R. Smith, and N. Kroll, “Negative refractive index in left-handed materials,” *Phys. Rev. Lett.*, vol. 85, p. 2933, 2000.

[9] R. A. Shelby, D. R. Smith, and S. Schultz, “Experimental verification of a negative index of refraction,” *Science*, vol. 292, p. 77, 2001.

[10] P. M. Valanju, R. M. Walser, and A. P. Valanju, “Wave Refraction in Negative-Index Media: Always Positive and Very Inhomogeneous,” *Phys. Rev. Lett.*, vol. 88, p. 187401, 2002.

[11] N. Garcia and M. Nieto-Vesperinas, “Is there an experimental verification of negative refraction yet?,” *Opt. Lett.*, vol. 27, p. 885, 2002.

[12] N. Garcia and M. Nieto-Vesperinas, “Left-Handed Materials Do Not Make a Perfect Lens,” *Phys. Rev. Lett.*, vol. 88, p. 207403, 2002.

[13] Andrew A. Houck, Jeffrey B. Brock, and Isaac L. Chuang, “Experimental Observations of a Left-Handed Material That Obeys Snell's Law,” *Phys. Rev. Lett.*, vol. 90, p. 137401, 2003.

[14] C. G. Parazzoli, R. B. Greegor, K. Li, B. E. C. Koltenbah, and M. Tanielian, “Experimental Verification and Simulation of Negative Index of Refraction Using Snell’s Law,” *Phys. Rev. Lett.*, vol. 90, p. 107401, 2003.

[15] M. Notomi, “Theory of light propagation in strongly modulated photonic crystals: Refractionlike behavior in the vicinity of the photonic band gap,” *Phys. Rev. B*, vol. 62, p. 10696, 2000.

[16] Chiyan Luo, Steven G. Johnson, J. D. Joannopoulos, and J. B. Pendry, “All-angle negative refraction without negative effective index,” *Phys. Rev. B*, vol. 65, p. 201104, 2002.

[17] S. Foteinopoulou, E. N. Economou, and C. M. Soukoulis, “Refraction in Media with a Negative Refractive Index,” *Phys. Rev. Lett.*, vol. 90, p.

107402, 2003.

[18] Ertugrul Cubukcu, Koray Aydin, Ekmel Ozbay, S. Foteinopoulou, and Costas M. Soukoulis, “Electromagnetic waves: Negative refraction by photonic crystals,” *Nature*, vol. 423, p. 604, 2003.

[19] E. Cubukcu, K. Aydin, S. Foteinopolou, C. M. Soukoulis, and E. Ozbay, “Subwavelength Resolution in a Two-Dimensional Photonic Crystal Based Superlens,” *Phys. Rev. Lett.*, vol. 91, p. 207401, 2003.

[20] Kaan Guven, Koray Aydin, K. B. Alici, C. M. Soukoulis, and Ekmel Ozbay, “Spectral negative refraction and point focusing analysis of a two-dimensional left-handed photonic crystal lens,” *Submitted to Phys. Rev. B*, 2004.

[21] E. Cubukcu, *Subwavelength Resolution in a Photonic Crystal Superlens*, Bilkent University M.Sc. Thesis, July 2003.

[22] J. B. Pendry, “Negative refraction makes a perfect lens,” *Phys. Rev. Lett.*, vol. 85, p. 3966, 2000.

[23] N. Seddon and T. Bearpark, “Observation of the Inverse Doppler Effect,” *Science*, vol. 302, p. 1537, 2003.

[24] Jie Lu, Tomasz M. Grzegorczyk, Yan Zhang, Joe Pacheco, Jr., Bae-Ian Wu, Jin A. Kong, and Min Chen, “Cerenkov radiation in materials with negative permittivity and permeability,” *Optics Express*, vol. 11, p. 723, 2003.

[25] Anthony Grbic and George V. Eleftheriades, “Experimental verification of backward-wave radiation from a negative refractive index metamaterial,” *J. Appl. Phys.*, vol. 92, p. 5930, 2002.

[26] M. C. K. Wiltshire, J. B. Pendry, I. R. Young, D. J. Larkman, D. J. Gilderdale, and J. V. Hajnal, “Microstructured magnetic materials for RF

flux guides in magnetic resonance imaging," *Science*, vol. 291, p. 849, 2001.

[27] Ekmel Ozbay, Koray Aydin, Ertugrul Cubukcu, Mehmet Bayindir, "Transmission and Reflection Properties of Composite Double Negative Metamaterials in Free Space," *IEEE Trans. Antennas Propag.*, vol. 51, p. 2592, 2003.

[28] Koray Aydin, Kaan Guven, L. Zhang, M. Kafesaki, C. M. Soukoulis, and Ekmel Ozbay, "Experimental Observation of True Left-handed Transmission Peak in Metamaterials," *To be published in Opt. Lett.*, 2004.

[29] Koray Aydin, Kaan Guven, and Ekmel Ozbay, "Observation of Negative Refraction and Negative Phase Velocity in Left-Handed Metamaterials", *Submitted to Appl. Phys. Lett.*, 2004.

[30] Charles Kittel, *Introduction to Solid State Physics*, John Wiley and Sons, New York, NY, 1996.

[31] J. D. Jackson, *Classical Electrodynamics*, John Wiley and Sons, New York, NY, 1962.

[32] C. M. Soukoulis(ed.), *Photonic Crystals and Light Localization in the 21st Century*, p. 351-371, Kluwer Academic Publishers, Netherlands, 2001.

[33] D. R. Smith, D. C. Vier, N. Kroll, and S. Schultz, "Direct calculation of permeability and permittivity for a left-handed metamaterial," *Appl. Phys. Lett.*, vol. 77, p. 2246, 2000.

[34] J. B. Pendry, and D. R. Smith, "Reversing light with negative refraction," *Phys. Today*, vol. 57, issue 6, p.37, 2004.

[35] D. R. Smith, D. Schurig, and J. B. Pendry, "Negative refraction of

modulated electromagnetic waves," *Appl. Phys. Lett.*, vol. 81, p. 2713, 2002.

[36] Mehmet Bayindir, K. Aydin, E. Ozbay, P. Markos and C. M. Soukoulis, "Transmission properties of composite metamaterials in free space," *Appl. Phys. Lett.*, vol. 81, p. 120, 2002.

[37] Richard W. Ziolkowski, and Ehud Heyman, "Wave propagation in media having negative permittivity and permeability," *Phys. Rev. E*, vol. 64, p. 056625, 2001.

[38] R. Marqués, J. Martel, F. Mesa, and F. Medina, "Left-Handed-Media Simulation and Transmission of EM Waves in Subwavelength Split-Ring-Resonator-Loaded Metallic Waveguides," *Phys. Rev. Lett.*, vol. 89, p. 183901, 2002.

[39] Nicholas Fang and Xiang Zhang, "Imaging properties of a metamaterial superlens," *Appl. Phys. Lett.*, vol. 82, p. 161, 2003.

[40] Kin Li, S. J. McLean, R. B. Greegor, C. G. Parazzoli, and M. H. Tanielian, "Free-space focused-beam characterization of left-handed materials," *Appl. Phys. Lett.*, vol. 82, p. 2535, 2003.

[41] M. Sanz, A. C. Papageorgopoulos, W. F. Egelhoff, Jr., M. Nieto-Vesperinas, and N. García, "Transmission measurements in wedge-shaped absorbing samples: An experiment for observing negative refraction," *Phys. Rev. E*, vol. 67, p. 067601, 2003.

[42] L. Ran, J. Huangfu, H. Chen, X. Zhang, K. Chen, T. M. Grzegorczyk, and J. A. Kong, "Beam shifting experiment for the characterization of left-handed properties," *J. Appl. Phys.*, vol 95, p. 2238, 2004.

[43] J. Huangfu, L. Ran, H. Chen, X. Zhang, K. Chen, T. M. Grzegorczyk, and J. A. Kong, "Experimental confirmation of negative refractive index

of metamaterial composed of Ω-like metallic patterns," *Appl. Phys. Lett.*, vol. 84, p. 1537, 2004.

[44] N. Katsarakis, T. Koschny, M. Kafesaki, E. N. Economou, and C. M. Soukoulis, "Electric coupling to the magnetic resonance of split ring resonators," *Appl. Phys. Lett.*, vol. 84, p. 2943, 2004.

[45] Richard W. Ziolkowski, "Superluminal transmission of information through an electromagnetic metamaterial," *Phys. Rev. E*, vol. 63, p. 046604, 2001.

[46] T. Weiland, R. Schuhmann, and R. B. Greegor, "Ab initio numerical simulation of left-handed metamaterials: Comparison of calculations and experiments," *J. Appl. Phys.*, vol. 90, p. 5419, 2001.

[47] C. Caloz, C.-C. Chang, and T. Itoh, "Full-wave verification of the fundamental properties of left-handed materials in waveguide configurations," *J. Appl. Phys.*, vol. 90, p. 5483, 2001.

[48] P. Markos, and C. M. Soukoulis, "Transmission studies of left-handed materials," *Phys. Rev. B*, vol. 65, p. 33401, 2001.

[49] P. Markos, and C. M. Soukolis, "Numerical studies of left-handed materials and arrays of split ring resonators," *Phys. Rev. E*, vol. 65, p. 36622, 2002.

[50] D. R. Fredkin and A. Ron, "Effectively left-handed (negative index) composite material," *Appl. Phys. Lett.*, vol. 81, p. 1753, 2002.

[51] P. Markos, I. Rousochatzakis, and C. M. Soukoulis, "Transmission losses in left-handed materials," *Phys. Rev. E*, vol. 66, p. 045601(R), 2002.

[52] J. Pacheco, Jr., T. M. Grzegorczyk, B.-I. Wu, Y. Zhang, and J. A. Kong, "Power Propagation in Homogeneous Isotropic Frequency-Dispersive

Left-Handed Media," *Phys. Rev. Lett.*, vol. 89, p. 257401, 2002.

[53] Jensen Li, Lei Zhou, C. T. Chan, and P. Sheng, "Photonic Band Gap from a Stack of Positive and Negative Index Materials," *Phys. Rev. Lett.*, vol. 90, p. 083901, 2003.

[54] I. V. Shadrivov, A. A. Sukhorukov, and Yu. S. Kivshar, "Beam shaping by a periodic structure with negative index of refraction," *Appl. Phys. Lett.*, vol. 82, p. 3820, 2003.

[55] R. W. Ziolkowski, "Design, Fabrication and Testing of Double Negative Metamaterials," *IEEE Trans. Antennas Propag.*, vol. 51, p. 1516, 2003.

[56] D. R. Smith and S. Schultz, P. Markos and C. M. Soukoulis, "Determination of effective permittivity and permeability of metamaterials from reflection and transmission coefficients," *Phys. Rev. B*, vol. 65, p. 195104, 2002.

[57] D. R. Smith and D. Schurig, "Electromagnetic Wave Propagation in Media with Indefinite Permittivity and Permeability Tensors," *Phys. Rev. Lett.*, vol. 90, p. 077405, 2003.

[58] T. Koschny, P. Markos, D. R. Smith, and C. M. Soukoulis, "Resonant and antiresonant frequency dependence of the effective parameters of metamaterials," *Phys. Rev. E*, vol. 68, p. 065602(R), 2003.

[59] T. Koschny, M. Kafesaki, E. N. Economou and C. M. Soukoulis, (*to be published in PRL*), 2004.

[60] M. M. Sigalas, C. T. Chan, K. M. Ho, and C. M. Soukoulis, "Metallic photonic band gap materials," *Phys. Rev. B.*, vol. 52, p. 11744, 1995.

[61] M. Bayindir and E. Ozbay, "Heavy photons at coupled-cavity waveguide band edges in a three-dimensional photonic crystal," *Phys. Rev. B*, vol. 62, p. R2247, 2000.

[62] A. Grbic, and G. V. Eleftheriades, “Overcoming the diffraction limit with a planar left-handed transmission-line lens,” *Phys. Rev. Lett.*, vol. 92, p. 117403, 2004.

[63] P. F. Loschialpo, D. L. Smith, D. W. Forester, and F. J. Rachford, and J. Schelleng, “Electromagnetic waves focused by a negative-index planar lens,” *Phys. Rev. E*, vol. 67, p. 025602, 2003.

[64] T. G. Mackay, A. Lakhtakia, “Negative phase velocity in a uniformly moving, homogeneous, isotropic, dielectric-magnetic medium,” *J. Phys. A: Math. Gen.*, vol. 37, p. 5697, 2004.

[65] O. F. Siddiqui, M. Mojahedi, and G. V. Eleftheriades, “Periodically loaded transmission line with effective negative refractive index and negative group velocity,” *IEEE Trans. Antennas Propag.*, vol. 51, p. 2619, 2003.